NIFS--92

JP9110105

H-mode Physics
–Experimental Observations and Model Theories–

Lecture Notes

Spring College on Plasma Physics, May 27 – June 21 1991
at International Centre for Theoretical Physics
(IAEA UNESCO)
Trieste, Italy

S.-I. Itoh

(Received – May 17, 1991)

NIFS-92 Jun. 1991

H-mode Physics -Experimental Observations and Model Theories-

Lecture Notes

Spring College on Plasma Physics, May 27 - June 21 1991
at International Centre for Theoretical Physics
(IAEA UNESCO)
Trieste, Italy

Sanae-I. ITOH
National Institute for Fusion Science, Nagoya 464-01 Japan

H-mode Physics -Experimental Observations and Model Theories-

Lecturer: Sanae-I. ITOH (National Institute for Fusion Science)
Chikusaku Nagoya 464-01 Japan

ABSTRACT

After the discovery of the H-mode in ASDEX (a tokamak in Germany) the transition between the L-mode (Low confinement mode) and H-mode (High confinement mode) has been observed in many tokamaks in the world. The H-mode has made a breakthrough in improving the plasma parameters and has been recognized to be a universal phenomena. Since its discovery, the extensive studies both in experiments and in theory have been made. The research on H-mode has been casting new problems of an anomalous transport across the magnetic surface. This series of lectures will provide a brief review of experiments for explaining H-mode and a model theory of H-mode transition based on the electric field bifurcation. If the time is available, a new theoretical model of the temporal evolution of the H-mode will be given.

Lecture 1: A Story of H-mode; L/H transition, H-phase, ELMs

By showing the experimental data of typical observations from 1982 to 1988, a picture of the H-mode is presented. Putting emphasis on the time scale and the causality between the observed phenomena in different places, the universal phenomena are extracted. For the onset of the L- to H- mode transition, necessary conditions are tried to be discriminated from the associated phenomena. Being identified the spatial regions, a story of H-mode (temporal evolution in various

phases) deduced from the experiments is given. A difficulty in applying the pioneering theories is clarified.

Lecture 2: A Model of H-mode transition; Bifurcation theory

From a story of experimental observations, key physics is to be extracted. The key physics variables are searched for, and the discovery of the missing link is shown. A new model theory of 1988 based on the bifurcation in the radial electric field is shown. By this mechanism, the particle and energy fluxes can have multiple values for the same density and/or temperature condition near the periphery. Successive experimental checks motivated by the bifurcation theories found the change in the electric field at L- to H- transition. Further observations in experiments and developments in the theory (1988-1990) are briefly compared and the improvements of the theory are shown. The transport problem associated with the H-phase is also given.

Lecture 3: A Model of ELMs, ELMy-H mode; Chaos and Mesophase

Temporal evolution of the H-mode in a diffusive media is considered. A new model equation for ELMs, ELMy-H mode from the extension of the bifurcation theory is given to be a time-dependent Ginzburg-Landau (TDGL) equation, which predicts the periodic oscillation of the edge density, an appearance of intermittent ELMs as well as chaotic oscillations. Mesophase of L phase and H phase exists near the edge region. If the time is available, this new topic will be discussed.

Key words: H-mode, L/H Transition, ELMs, Theoretical models, Experimental observations, Review

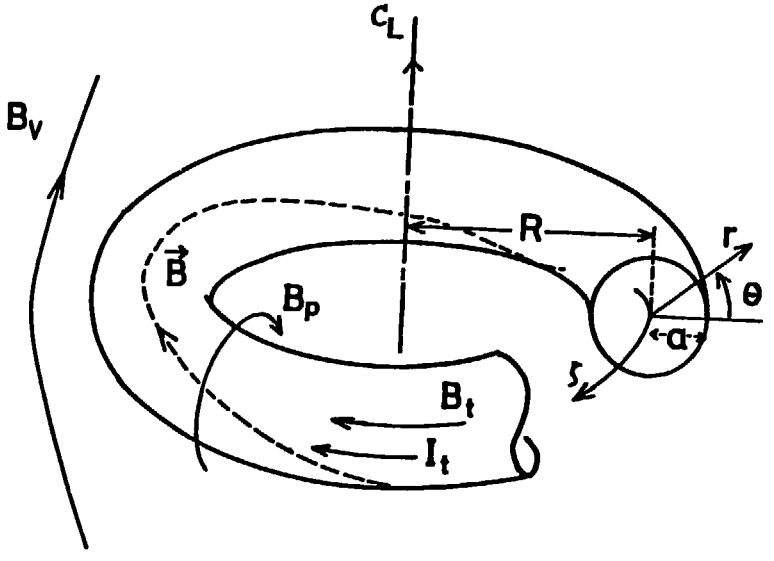
C_L
B_V
R
r
θ
a
$\vec{B}$
B_p
B_t
I_t
ζ

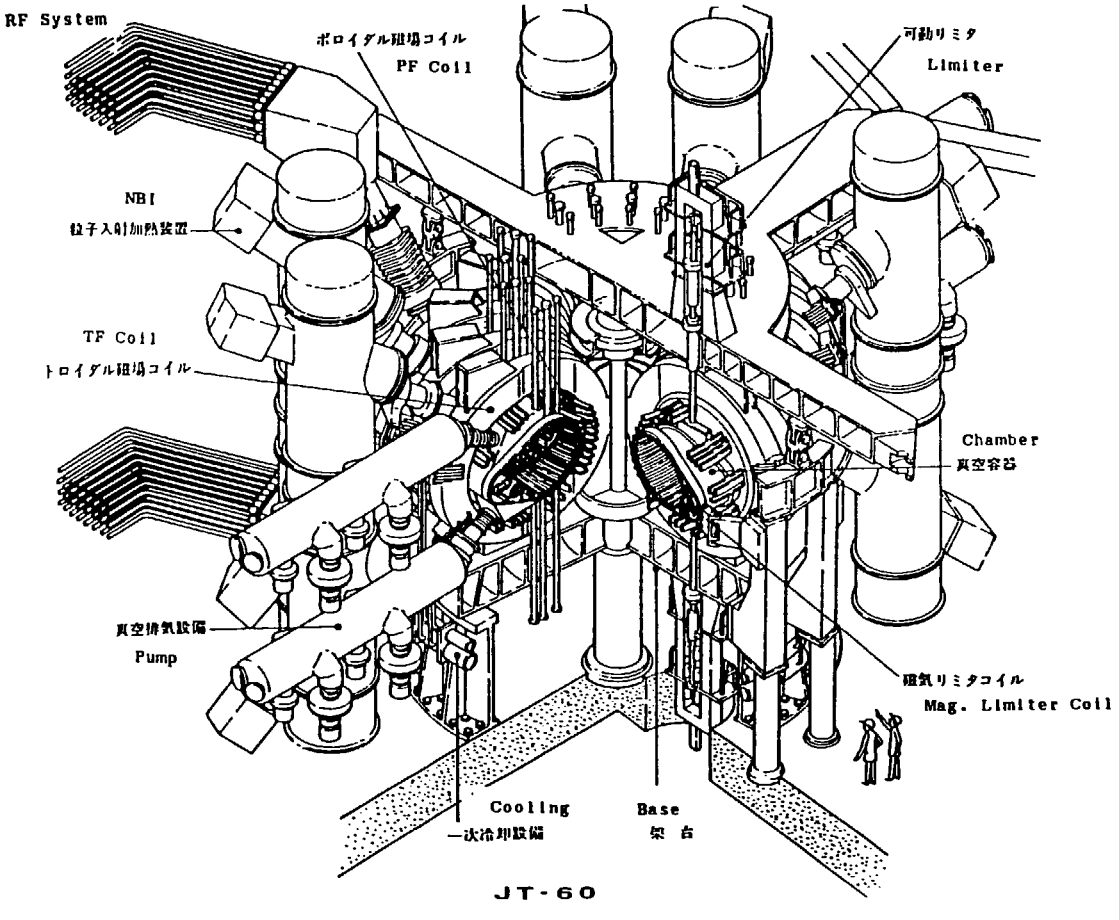
RF System
ポロイダル磁場コイル
PF Coil
可動リミタ
Limiter
NBI
粒子入射加熱装置
TF Coil
トロイダル磁場コイル
Chamber
真空容器
真空排気設備
Pump
磁気リミタコイル
Mag. Limiter Coil
Cooling
一次冷却設備
Base
架 台
JT-60

Lecture 1

-- devices, experimental results, physics quantities, place, time, causality, inter-relations, etc.

Introduction to tokamaks

1) The H-mode is the name of a typical discharge in tokamaks with high confinement properties. Before beginning the story of the H-mode, let us briefly explain the tokamak device and its magnetic and topological configuration. The schematic bird's-eye drawing is shown in Figure. Magnetic configuration is mainly determined by the external magnetic coil systems and the plasma current inside the vessel. The concept of tokamak configuration is developed in USSR by Acad. Artimovich and now considered to be the most promising candidate for a fusion reactor system. The future world-wide plan of the device called International Thermonuclear Experimental Reactor (ITER) is based on this machine configuration.

2) There are many tokamak devices in the world. Here we show the overview of the some machines. They are JET, the largest machine in the world which is operated by CEC and is located in England, JT-60, the machine in Japan Atomic Energy Research Institute and the ASDEX in Germany, in which the H-mode was first discovered by Dr. Wagner.

3) In the operation, the high temperature plasma is firstly obtained by ohmic discharge with the aid of and external

ITER REFERENCE PARAMETERS

Plasma major radius, R (m)	6.0
Plasma half-width at midplane, a (m)	2.15
Elongation, 95% flux surface	1.98
Toroidal field on axis, B_o (T)	4.85
Nominal maximum plasma current, I_p (MA)	22
Nominal fusion power, P_f (MW)	1000

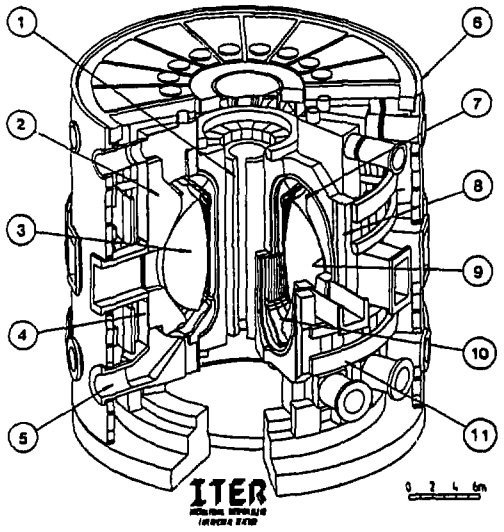

1- CENTRAL SOLENOID
2- SHIELD/BLANKET
3- PLASMA
4- VACUUM VESSEL-SHIELD
5- PLASMA EXHAUST
6- CRYOSTAT
7- ACTIVE CONTROL COILS
8- TOROIDAL FIELD COILS
9- FIRST WALL
10- DIVERTOR PLATES
11- POLOIDAL FIELD COILS

The ITER NEWSLETTER is prepared and published by the International Atomic Energy Agency, Wagramerstrasse 5, P.O. Box 100, A-1400 Vienna, Austria. Telex: 1-12645, Cable: INATOM VIENNA. Facsimile: 43 1 234 564. Tel.: 43 1 2360-8393/8394. Items to be considered for inclusion in the ITER Newsletter should be submitted to B. Kouvchinnikov, ITER Secretariat.

Printed by the IAEA in Austria
March 1991

91-00845

JET

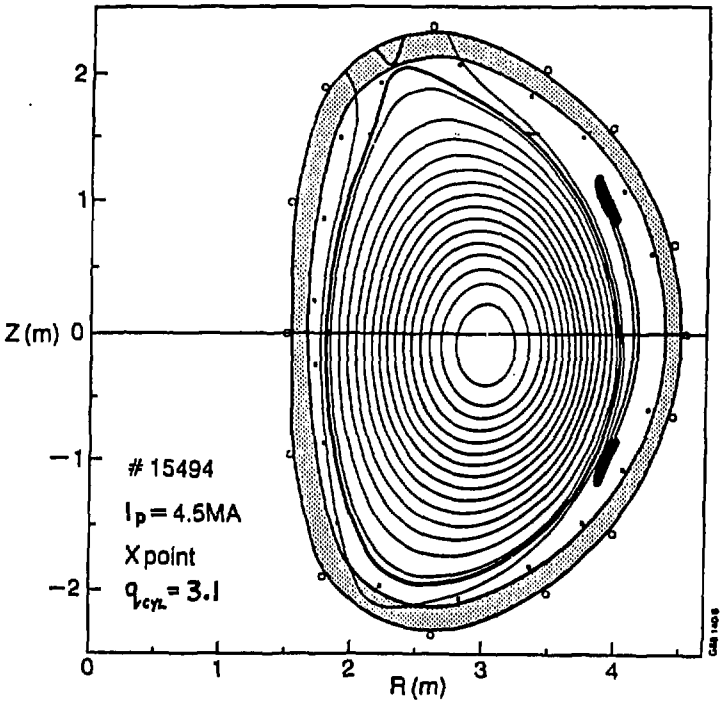

magnetic flux supply, and with additional heating method like neutral beam injection (NBI) and/or radio-frequency wave heatings (ICRF, ECRF, LHRF), the systems are seen in the preceding view-graphs. For the understanding the situation and the location of the external systems, the graphical drawing of the bird's-eye view of the JT-60 tokamak in Japan is shown, which is one of the three large tokamaks in the world and the configuration has been re-modeled recently.

4) Inside view of the machine is also shown for JET, JT-60. The International Thermonuclear Experimental Reactor (ITER) is also shown.

5) Here we show a picture of the discharge on the poloidal cross-section which was taken in ASDEX. The pattern shows so-called a double nulls(DN) configuration. In the top and bottom of the central plasma, two X-points, corresponding to double nulls, are seen. Inside the plasma, we experimentally observe the pressure profiles, such as the density profile and the temperature profile, as functions of the magnetic surface. In other word, the physics quantities are often interpreted as a function of magnetic surface, which is illustrated in the next viewgraph.

Outside the separatrix, we also observe a low density plasma, which is called scrape-off layer (SOL). The magnetic surface is shown for the single null configuration in JFT-2M of Japan Atomic Energy Research Institute.

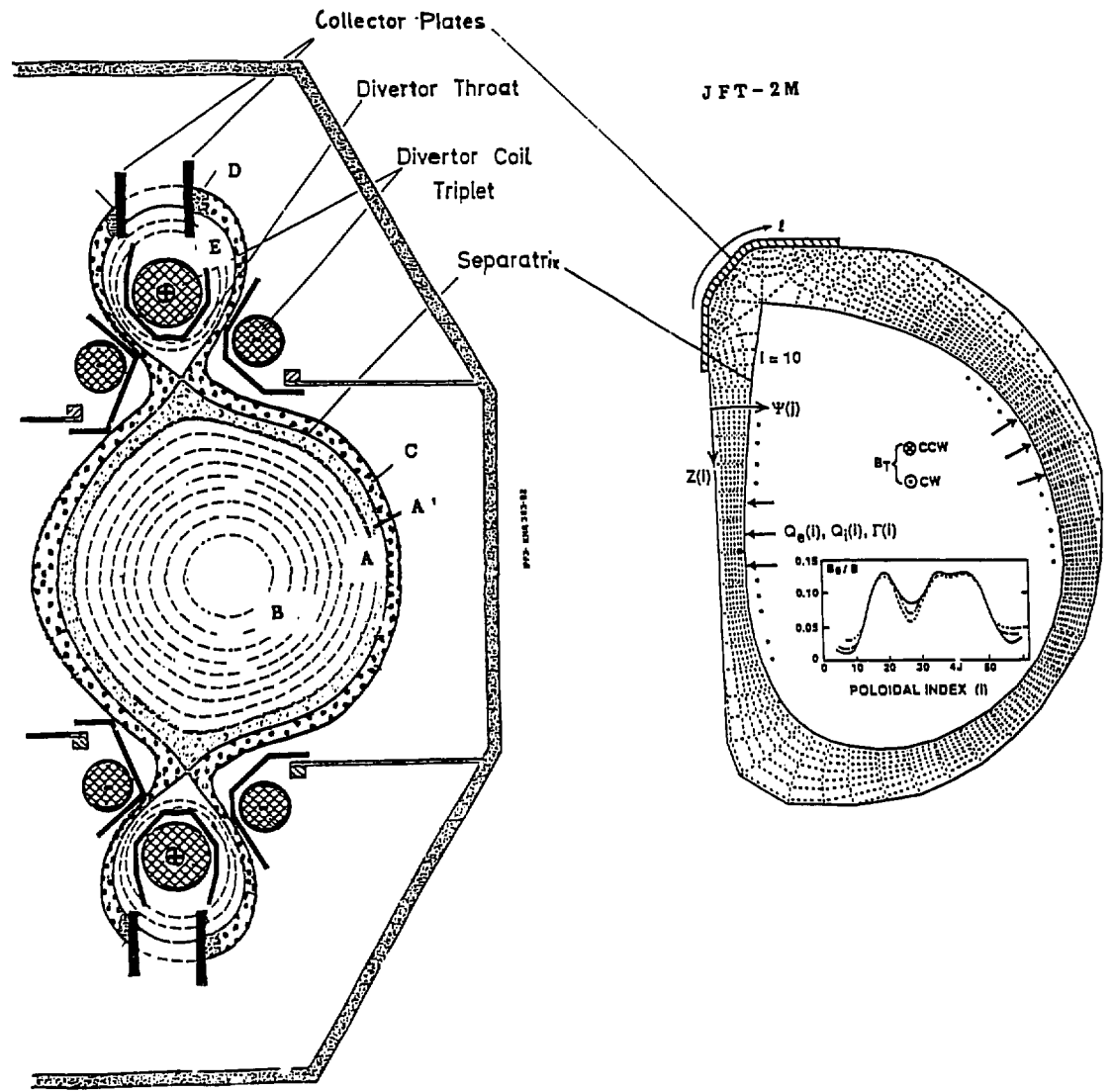
ASDEX
Collector Plates
Divertor Throat
Divertor Coil
Triplet
Separatrix
D
E
C
A'
A
B
JFT-2M
l
l = 10
Ψ(l)
Z(l)
B_T ⊗CCW ⊙CW
$Q_e(l)$, $Q_i(l)$, $\Gamma(l)$
B_θ/B
0.15
0.10
0.05
0
10
20
30
40
50
POLOIDAL INDEX (l)

6) The contour of the magnetic surface and the schematic configuration of the vacuum vessel as well as the divertor chamber is illustrated for the ASDEX. This configuration is called to be an closed divertor configuration. If there is no baffle or the shielding fence between the main chamber and the divertor, the configuration is called to be open. (recall the difference between the JET-inside and ASDEX-inside)

In the following, we discuss the places of the observed phenomena during the discharge using this contour pattern. The locations of the plasma center, edge region, mid-plane, the outer-most magnetic surface, the separatrix surface, the scrape-off layer (SOL), the divertor chamber, the divertor plates, and so on are shown.

7) We start with the typical H-mode discharge obtained in ASDEX. On *the H-mode*, there is a good and extensive article published in Nuclear Fusion as a special topic by ASDEX Team. (Nucl Fusion, *29* NO.11 (1989) 1959-2040) Mainly following the experimental observations presented in this article, let us consider the H-mode.

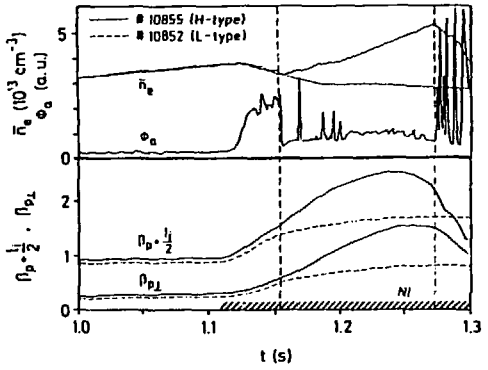

FIG. 1. Variation of the line averaged density $\bar{n}_e$, the atom flux ϕ_a from the outer neutralizer plate at the intersection of the separatrix and the neutralizer plate, $\beta_p + \ell_i/2$ from the plasma equilibrium and $\beta_{p\perp}$ from the diamagnetic signal, during a neutral injection (NI) pulse (hatched area). Compared are an H-discharge (solid lines) and an L-discharge (dotted lines). The L–H transition is indicated by the dashed vertical line. The two discharges differ only in the current, which is 300 kA in the L-discharge and 275 kA in the H-discharge.

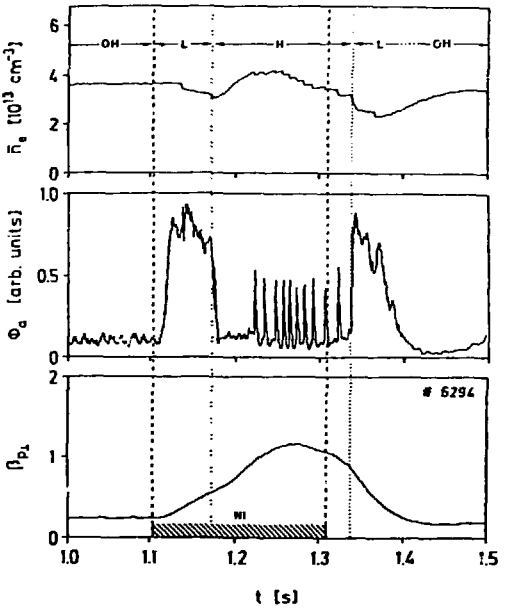

FIG. 3. Variation of the line averaged electron density $\bar{n}_e$, the atom flux ϕ_a from the outer neutralizer plate at the intersection of the separatrix and the neutralizer plate, and $\beta_{p\perp}$ from the diamagnetic loop during the NI phase (hatched area) and during the H- and L-phases.

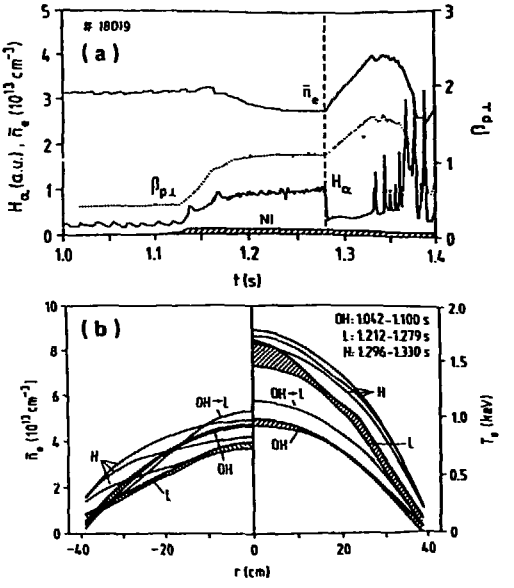

FIG. 2. (a) Electron density $\bar{n}_e$, $\beta_{p\perp}$ and H_α radiation in the divertor chamber; the L–H transition is indicated by the dashed vertical line. (b) Development of the electron temperature and density profiles from the Ohmic phase to the L- and H-phases.

8) Typical H-mode discharges, (Fig. no. 1,2)

variation of the line averaged density n_e

the density increases after the onset of H-mode

β value (plasma pressure/magnetic pressure)change

β value increases

the atom flux from the outer neutralizer plate Φ_a

(the measure of the particle flux to plate)

sudden decrease of the particle flux to the plate

typical parameters of H-mode in ASDEX

R $\sim$ 165cm, a $\sim$ 40cm, B_T=1.5 - 2.8T, I_p=.18 -.45kA,

others are seen in figures

Compare with the L-mode discharge

9) The spontaneous transition to H-mode is seen in the Figs. With a preceding L-phase, the H-mode takes place and lasts after the termination of NBI. (Fig. no. 3)

During the H-phase, Edge Localized Mode (ELM) as revealed as the spikes of Φ_a to divertor appears.

Φ_a

corresponding to the particle flux to the divertor plate

An occurrence of H-mode transition and the short H-phase is seen even in the phase of the post NBI pulse. (Fig. no. 71)

Note that when the edge electron temperature reaches the critical value, the transition occurs, T_e?

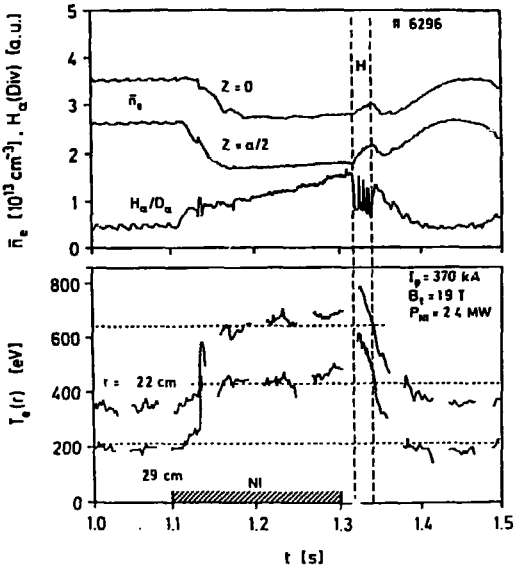

FIG. 71. Line averaged density at the plasma centre (z = 0) and along the chord z = a/2, H_α/D_α radiation in the divertor chamber, and electron temperature at two radial positions. The H-phase (between dashed lines) occurs after switching on the NI pulse during a phase of elevated temperature.

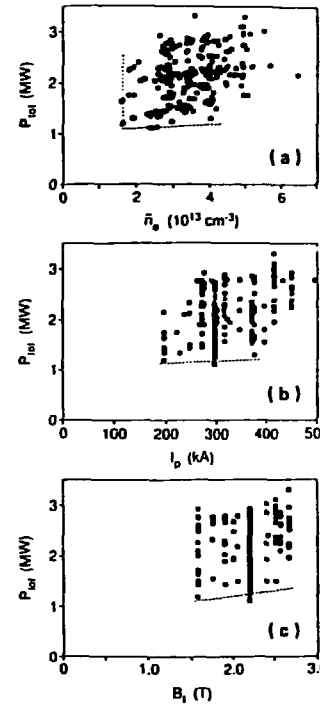

FIG. 54. Operational diagram for H-mode plasmas giving the power threshold versus (a) line averaged density $\bar{n}_e$, (b) plasma current I_p and (c) toroidal field B_t.

JET

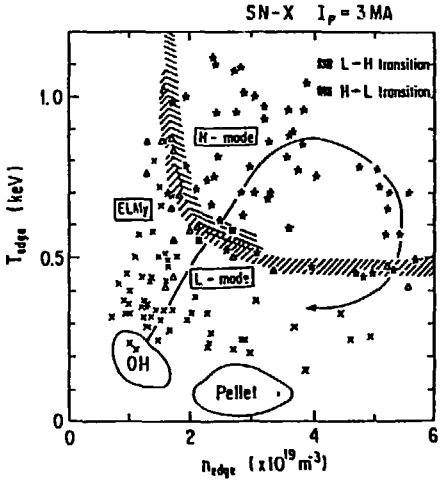

JT-60

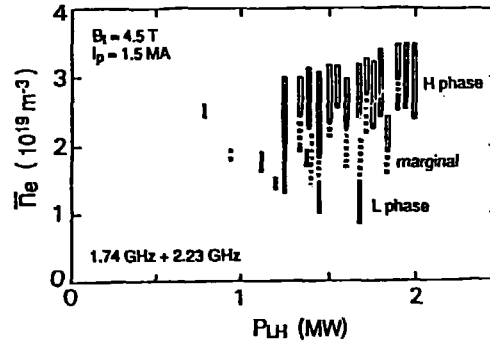

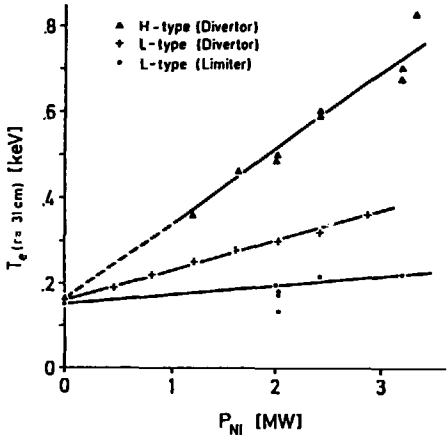

FIG. 70. Variation of the edge electron temperature with the beam power in limiter discharges and in L- and H-type divertor discharges. I_p = 0.38 MA, $\bar{n}_e \simeq 3 \times 10^{13}$ cm^{-3} (H), $\bar{n}_e \leq 2 \times 10^{13}$ cm^{-3} (L) and $\bar{n}_e \simeq 5 \times 10^{13}$ cm^{-3} (limiter).

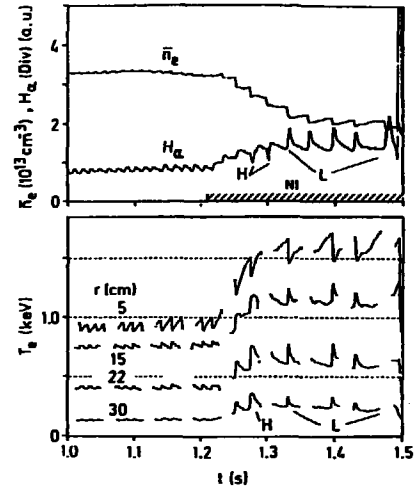

FIG. 73. Line averaged density, H_α radiation in the divertor chamber, and ECE electron temperature during an L-discharge with large sawteeth. Two sawteeth give rise to a short H-phase.

ASDEX TEAM

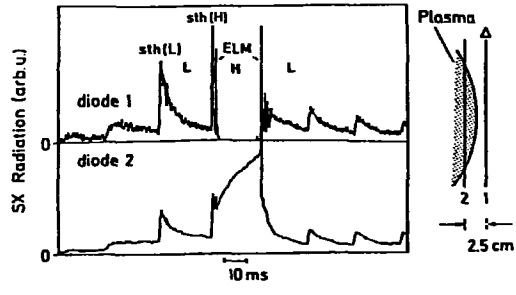

FIG. 74. Soft X-ray radiation during the L-phase with large sawteeth. Diode 1 views the SOL, diode 2 views mainly the plasma within the separatrix. One sawtooth, sth(H), gives rise to a transient H-phase.

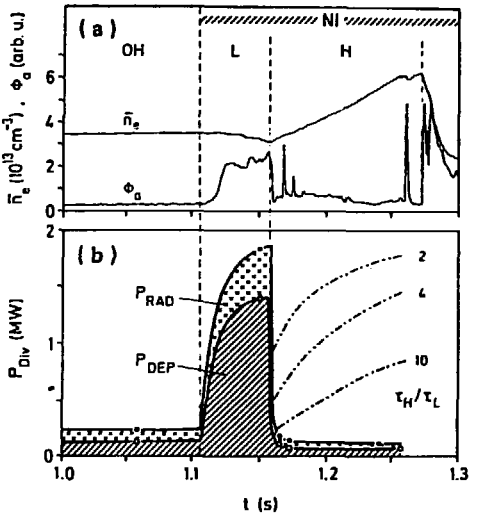

FIG. 37. Time development of (a) $\bar{n}_e$ and Φ_a, and (b) the total power flow P_{Div} into the divertor chambers. The dash-dotted lines show the variation of the normalized transport losses for energy confinement time changes at the L–H transition (I_p = 0.315 MA, P_{NI} = 3.5 MW).

ASDEX TEAM

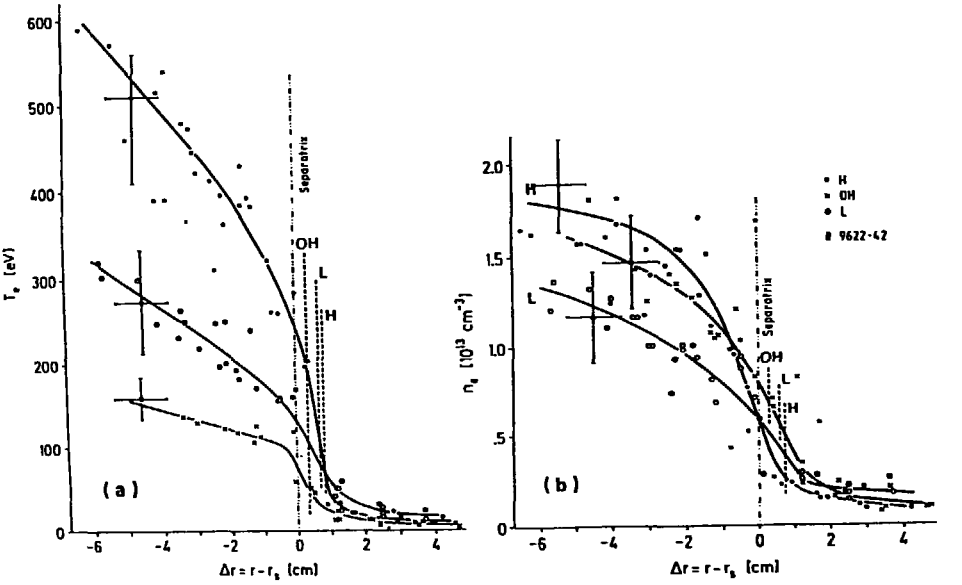

FIG. 28. Radial profiles of (a) T_e and (b) n_e, in the midplane over the separatrix, for ohmically heated and beam heated discharges; $r = r_s$ is the nominal separatrix position according to magnetic signals. Vertical bars indicate separatrix positions determined from electron pressure profiles in the divertor chamber using the assumption that n_eT_e = constant along field lines. The question of the exact location of the separatrix is discussed in the text.

10) Existence of the threshold for the L/H transition
(Fig. no. 54 & JET & JT-60)

Threshold power P_{th}
Threshold averaged density n_e
for the onset of H-mode transition (ASDEX, JT-60)

Threshold edge temperature T_{edge}
Threshold edge density n_{edge}
for discriminating L, H modes (JET)

11) The relation between the input power and the edge temperature, P_{in} - T_{edge}, is seen for various discharges.
The threshold power can be interpreted as the threshold edge temperature (Fig. no. 70)

Critical temperature for the transition?
Sawteeth trigger Short H phase (Fig. no. 73)

*Critical density, temperature or pressure?

What happens inside and outside the plasma?

12) Formation of the transport barrier
temporal soft x-ray signals from diode 1 and 2
(the width between 1 & 2 is 2.5cm) (Fig. no. 74)

Sudden reduction of the power and particle fluxes to the divertor region (Fig. no. 37)
P_{rad} power radiated in the divertor chamber,
P_{dep} power deposited to the chamber
Particle flux barrier Φ_a

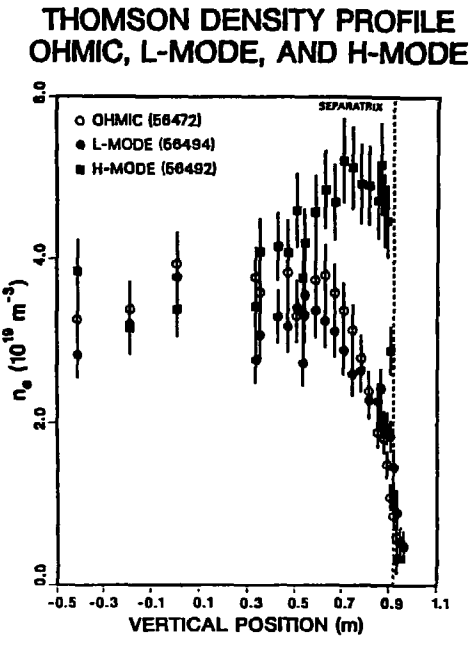

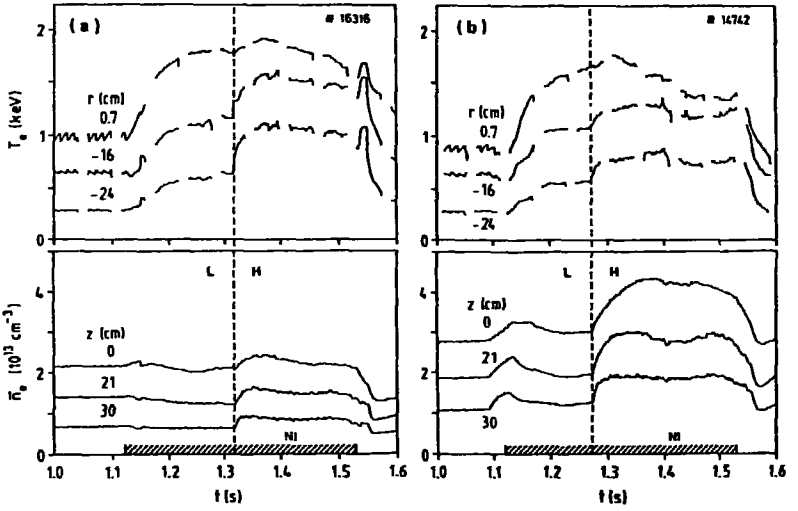

FIG. 6. Time evolution of the electron temperature T_e and the line averaged density $\bar{n}_e$ at three positions during the beam heating phase with L-H transitions (dashed vertical line).
In case (a), the density is regulated by a feedback system; in case (b), the internal gas flux is increased just before the beam is switched on and is then maintained at a constant level. The breaks in the electron cyclotron emission traces are caused by a chopper which is used to monitor possible drifts in the background signal.

13) Steep edge gradients of density and temperature
Pedestal formation on the plasma profile

temperature pedestal ASDEX (Fig. no. 28)
density pedestal or hollow profile D-III-D
(above Fig. no. 6)

temperature/density -- closed/open div. ASDEX

14) Temperature rise from the edge -closed divertor
Density rise near the edge -open divertor
(Fig. no. 6) neutral effect?
Different temporal evolutions in the density and temperature profiles Gradual change of β

15) The changes in the confinement properties

Temporal evolution of transport coefficients
(particle diffusivity at the edge convection)
global heat conductivity (χ_e vs χ_i) (Fig. no. 40)
profiles of χ_e & χ_i change
plasma toroidal rotation profile (Fig. no. 43)
fluctuations edge vs core

16) Temporal evolution of the pressures β_{dia},
(Fig. no. 9 of Ref.3)

electron pressure profile development,
ELM activities,
pedestal formation and relaxation
the associated bursts

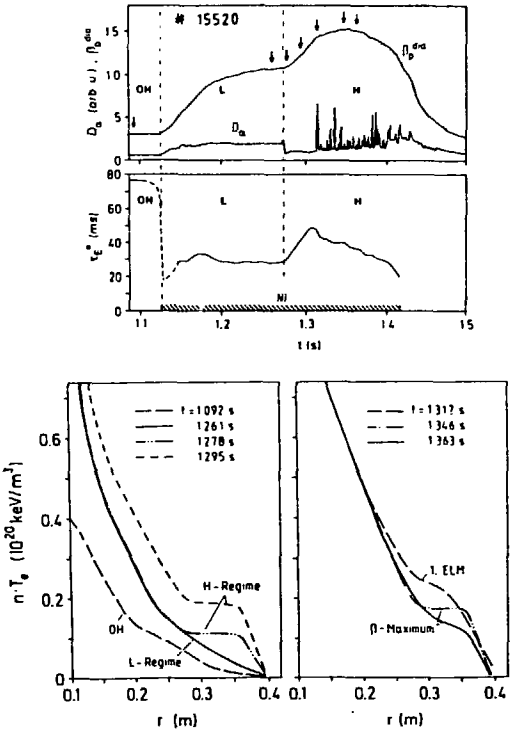

Fig. 9. Diamagnetic beta β_p^{dia}, H_α-light intensity and energy confinement time $\tau_E^* = W/(P_{tot} - dW/dt)$ (top) together with profiles of electron pressure $n \cdot T_e$ at characteristic times (bottom) of an H-mode β-limit discharge ($I = 310$ kA, $\bar{n}_e = 3.4 \times 10^{13} cm^{-3}$, $P_{NI} = 3.5$ MW, $H^0 \rightarrow D^+$).

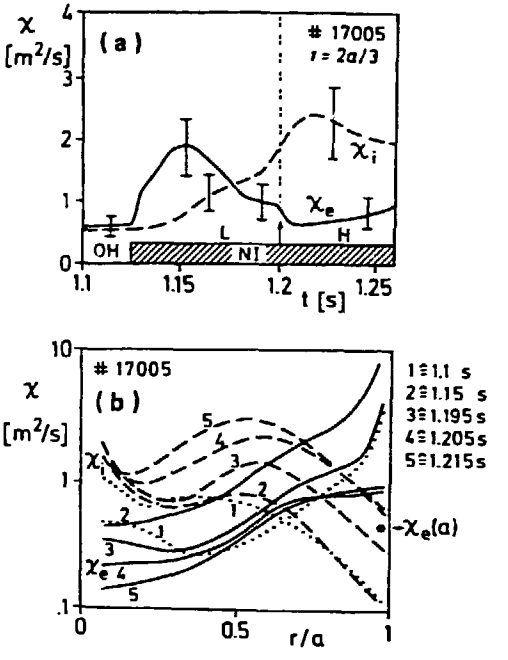

FIG. 40. (a) Electron diffusivity χ_e and ion heat diffusivity χ_i ($= \chi_{i,NC} + \chi_i, \eta_i$) versus time during consecutive OH-, L- and H-phases of a $D^0 - D^+$ discharge.
(b) Corresponding radial profiles of χ_e and χ_i in the Ohmic phase (1), the L-mode (2) and at the L-H transition (3–5). The dots denote $\chi_e(a)$ deduced from the profiles of Fig. 28 in a quiescent H-phase.

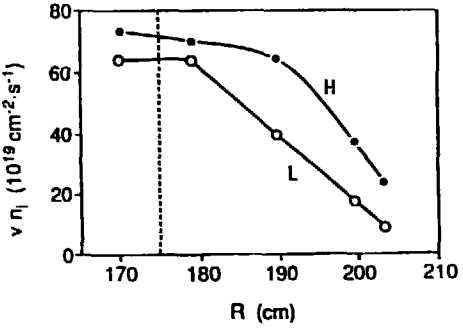

FIG. 43. Momentum profiles in the L- and H-phases measured by resonant charge exchange on O^{7+}.

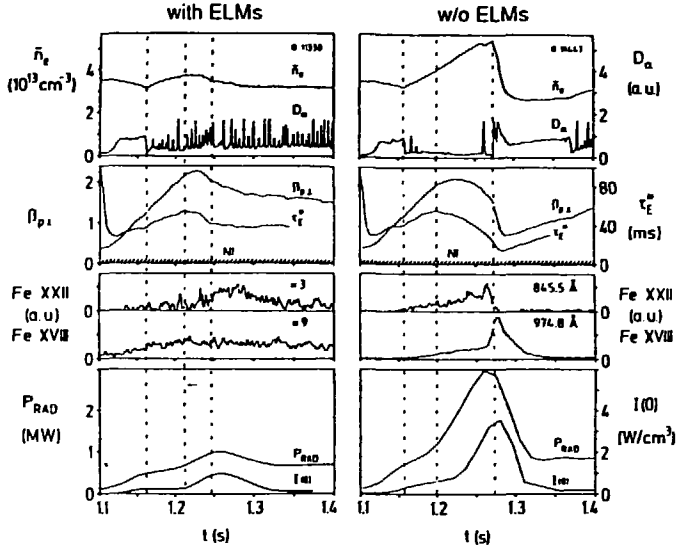

FIG. 23. Time evolution of various plasma parameters of H-mode discharges with and without ELMs (I_p = 0.32 MA, B_t = 2.17 T, P_{NI} = 3.3 MW, $H^0 - D^+$): line averaged plasma density $\bar{n}_e$, D_α light intensity in the divertor chamber, poloidal beta β_p, global energy confinement time τ_E^*, Fe XVIII and Fe XXII line intensities (representative of iron radia ion from r/a = 2/3 and from the plasma centre, respectively), and total and central radiation losses P_{RAD} and I(0).

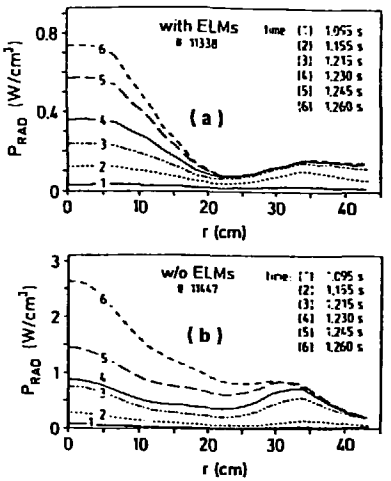

FIG. 24. Radiation power density profiles of (a) an ELM dominated H-discharge and (b) an ELM free H-discharge.

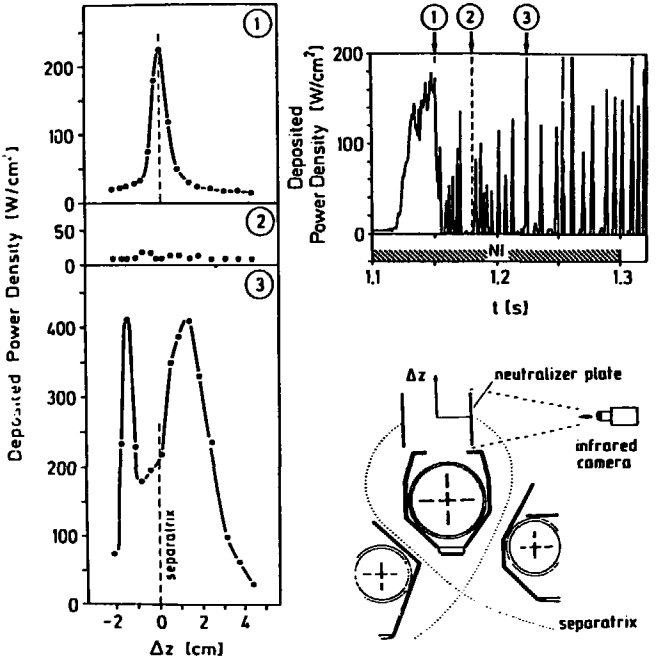

Fig. 5. Profiles of deposited power density onto the neutralizer plates during different NI-phases: (1) L-phase, (2) quiet H-phases between bursts, and (3) at a burst. For comparison, the H_α/D_α divertor radiation is shown. Δz is the distance from the intersection of separatrix and neutralizer plate. $I_p = 320$ kA, $\bar{n}_e = 4\times10^{13}$ cm^{-3}, $P_{NI} = 2.85$ MW.

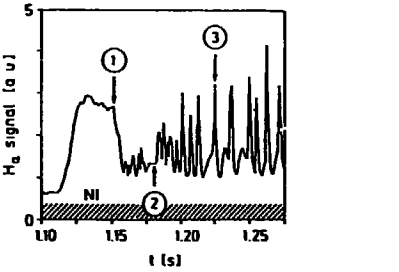

1 t = 1.15 s
2 t = 1.181 s
3 t = 1.225 s

a FWHM = 0.8 cm
b FWHM = 0.7 cm
c FWHM = 2.7 cm

9598

17) Temporal evolutions of the plasma parameters

with ELMs and ELM-free,
continuous density increase
impurity increase
radiation power increase
radiation collapse, termination of H-phase

Transient behaviour - not steady

18) Temporal evolution of the radiation profiles

with ELMs and ELM-free H-mode (Fig. no. 23)
edge radiation vs central radiation
absolute value (Fig. no. 24)

*In the early stage, the temporal evolution is not known
the radiation is one candidate for the onset of H-mode.

19) ELM bursts at divertor

Deposited power density onto the plate
(Fig. of Ref.5)
(L-phase, H-phase, ELM burst)
Temporal evolutions of power density and H_α
(Fig. no. 5 of Ref.4)

problems casting to particle exhaust, heat removal
transient heat load, ash (impurity)

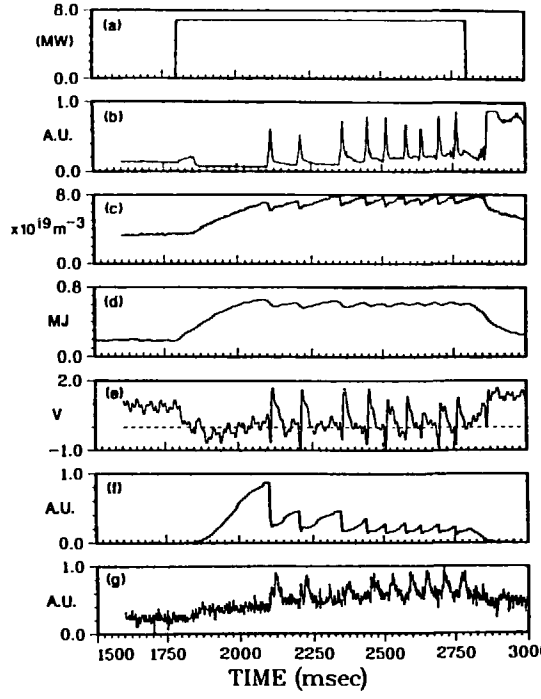

FIG. 1. Time histories from a typical *H*-mode discharge with giant ELM's for 1.25-MA plasma current, 2.1-T toroidal field, NBI power of 6.8 MW, (a) NBI power, (b) D_α emission in the divertor region, (c) line-averaged electron density, (d) plasma stored energy, (e) loop voltage, (f) edge soft x-ray emission, and (g) edge visible bremsstrahlung.

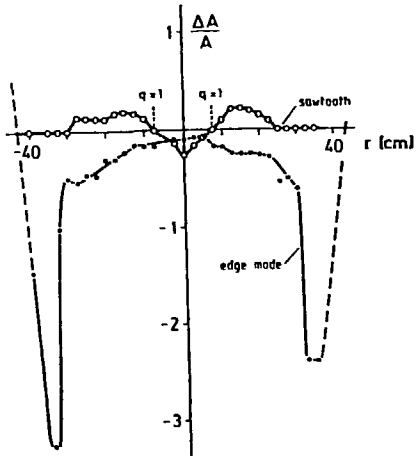

FIG. 17. Radial distributions of soft X-ray fluctuations connected with an ELM and a sawtooth. The measurements indicate that the ELMs are localized at the plasma edge.

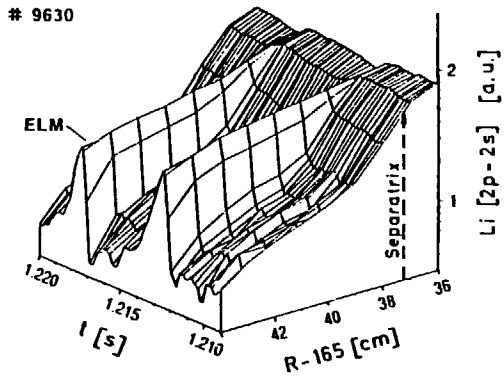

FIG. 18. Three-dimensional plot of the Li [2s–2p] light intensity along the beam over the period 1.209-1.22 s, encompassing two ELMs.

20) Temporal evolution of edge impurity contamination during a repetitive ELMs. (Giant ELMs in D-III-D)
(Fig. no. 1 of Ref.19 a)

Impurity accumulation vs ELM activity
a cause or an associated phenomena of ELMs?

21) Radial structure of Edge Localized Mode soft X ray fluctuation
(Fig. no. 17)

Temporal structure of ELM burst activities
(Fig. no. 18)

22) After seeing the experimental observations, we would like to ask ourselves what the key issue to dictate the H-mode is. Let us consider the phenomena dividing the problems into four.

1 : What is the necessary condition for the H-mode?
discrimination of the universal facts from the associated phenomena,
what are the machine dependent quantities,
what kind of inter-relation between the physics variables is expected.

2 : Considering the temporal evolution of the H-mode as ;
L/H transition, H-phase, occurrence of ELM activities and the termination,
what processes happen in each phase
what governs the each state and duration?

3 : Is the H-mode compatible to external control systems,
heating method, particle supply and exhaust,
heat removal and so on?
Is the H-mode consistent with the operating scenario as the fusion core?

4 : What are the future prospect and problems to be solved?

Summarizing the experimental observations, we may see the following facts for the H-mode life. 23)

1. Necessary conditions for the onset of L/H transition.

There is a threshold power level (P_{th}) for the plasma parameters so as to satisfy the condition of a spontaneous transition.

The transition is possible with any kind of the heating methods including the ohmic heating alone.

Finite time ($\sim\tau_E$) from the start of additional heating is necessary for the onset of the transition. (L-phase)

The transition is possible regardless of the existence of separatrix, i.e., in both divertor and limiter configurations.

The threshold power level can be reduced by the following changes. However, if the transition takes place, these differences do not so affect the characteristics of H-phase, e.g., τ_E.

a) Ion gradient-B drift is toward the X-point.
b) The distance between X-point and bad (magnetically) curvature region is long.
c) The distance between the plasma surface (boundary) and the limiter is wide.
d) preferential edge heating to the central core heating.
e) The existence of heat and particle flux from the core due to the sawteeth.
f) Edge cooling due to impurity radiation is smaller.
g) Neutral gas pressure around the main plasma is low.
h) The safety factor q is smaller.

i) Both the total plasma current and the toroidal magnetic field strength are low.

j) Toroidal rotation is co-direction to the plasma current direction.

The transition condition alters for the different gaseous species and depends on charge and/or mass.

2. L to H transition 24)

Edge electron temperature and/or density and/or their gradients reach the threshold values for the transition.

Just inside the separatrix, the transport barrier is formed and the sudden decrease of the particle and heat outfluxes across the plasma boundary takes place.

The fluxes to the divertor plate also suddenly decrease.

The magnetic fluctuation observed in scrape-off layer (SOL) decreases.

3. H-phase, temporal evolution after the transition

After the transition, the steepening of the density and/or temperature gradients starts just inside the separatrix.

The pedestal formation in the electron temperature profile occurs. In the large devices, the electron density profile tends to be hollow.

The global energy confinement time τ_E gradually increases according to the time scale of the electron temperature rise.

The confinement time τ_E in H-phase is twice as large as that in L-phase. Up to 1987yr, the dependence was not clear.

(ITER activity gathered the H-mode database and obtained the scaling in 1990. The article will be published in forthcoming issue of Nuclear Fusion in 1991.)

The reduction or annihilation of sawteeth activities are sometimes observed. The fact may imply the flattening of the current profile.

4. Impurity accumulation and Occurrence of ELMs [25]

Impurity accumulation takes place in the time scale similar to the energy confinement time τ_E.

Bursts due to ELM (Edge Localized Mode) are often observed. The bursts consist of the particle flux, the heat flux and the amplitude of magnetic fluctuations.

ELMs suddenly exhaust the particle and heat from the pedestal part of the plasma edge away to SOL region. Then the decreases of the density and the temperature propagate to the core region.

The magnitude and the frequency of ELMs depend on the configuration, the species of the gas, impurity, input power, toroidal rotation and so on. Details are not known.

Without bursts due to ELMs, the density increase and the impurity accumulation continue and the quasi-steady state can not be obtained. Finally the H-mode discharge meets the radiation collapse, or reaches the critical β and degraded confinement.

5. H to L transition

The reduction of the heat flux (not the input power) across the plasma boundary causes H- to L transition.

When the central radiation loss overcomes the input power $P_{rad} > P_I$, or with the delay time ($\sim\tau_E$) after the termination of the heating, it occurs.

The edge temperature just before the H to L transition is lower than that just before the L to H transition.

The transition sometimes associates the burst of H_α/D_α light, which is similar to ELM's burst.

Lecture 2

---A model of H-mode transition, bifurcation theory

There has been several theoretical work on modeling the H-mode, the transition characteristics have not been fully explained. The transition occurs in both the separatrix and limiter configurations, and is originated from the change of the transport inside the outermost magnetic surface. There must be a critical condition for the electron temperature and/or density, and/or their gradients, near the edge. At the onset of the transition, the heat flux which is going out of the plasma surface, P_{out}, suddenly reduces while the temperature and density remain almost unaltered. A finite time is necessary for the change of the background plasma parameters.

1) In order to make a model theory of the H-mode let us first review the experimental context in Lec.1. To identify the location of each phenomena during the life of the H-mode, the region of the plasma is divided into five. (A: edge region, (A'⊆A): edge just inside the separatrix, B: core region, C: outside the separatrix surface (SOL), D: divertor region outside of the separatrix, E: divertor region inside the separatrix. (shown in the viewgraph)

*Necessary conditions in L-phase

The H-mode life starts with L-phase and the conditions and constraints are determined by the transport in the L-phase. The necessary conditions of the plasma parameters in A & A' for the onset of the H-mode transition is given in the L-phase period. For example, the temperature at A' (T_{edge} & ∇T_{edge}) is influenced by the P_{in}-P_{out}, where P_{in} is the input power to regions A & B and P_{out} is the heat outflux from A' to C, the

impurity radiation loss in region A'(& A), the width of C layer and other transport processes in A (B) and C,D. The remark on P_{th} is necessary.

2) *L to H transition

The bifurcation of the flux occurs at A'. When T_{edge} or ∇T_{edge} exceeds a certain threshold value, P_{out} suddenly decreases and the transport barrier is established. The change of T_{edge} or ∇T_{edge} at the transition is small. These experimental observations suggest that the transition should have a property that the heat and particle fluxes have two or multiple values for one condition of the temperature and density. The radial electric field is a candidate to play the role to cause such a transition as a hidden variable.

*Steep gradient and Pedestal formation

The sudden decrease of P_{out} and Γ_{out}, Γ_{out} is the particle out flux, make the fall-off lengths of the temperature and density in C (SOL) be short, and reduce the neutral particle recycling. Simultaneously the sudden increase of the heat flux to A', P_{in}-P_{out} occurs and the formation of steep gradient with the pedestal starts.

*Increase of Energy confinement (τ_E)

The increase of density and temperature in A propagates to B. The higher pressure profile with the pedestal near edge is obtained.The electron thermal conductivity χ_e reduces. The density profile becomes broad. The current profile is expected to be broad too. The sawtooth activity reduces and low-m tearing (global MHD)mode tends to be stabilized. Due to the steep gradient in A', the impurity accumulation starts.

3) *ELMs

The ELM activity is observed in A'. The particle and heat in the pedestal A' are exhausted in the form of bursts. The burst also contains the fluctuating part of magnetic field. Whether the ELMs is the origin of the magnetic fluctuation in C or not is not known. After the burst, the pedestal formation starts again. The period, the duration and the amplitude of ELMs have varieties. Details are searched for. Without a ELM activity, the radiation in B increases and goes to collapse. The collapse occurs due to the strong density increase even in the absence of an impurity accumulation.

*H to L transition

This may be a reverse process of L to H transition. Whether this is a kind of ELMs, which can not return to H phase, or not is still a question. The cause and the place of this transition are not yet fully understood.

The key issue to understand the H-mode is the mechanism of the L- to H- mode transition. The region is identified to be the plasma edge.
--- Previous model theories in which the origin of the transition is found in SOL show the difficulty.

Let us firstly show a possible mechanism of the L-to H-mode (H- to L-mode) transition associated with the changes in the particle flux and the convective energy loss near the plasma edge. Bipolar ion loss near the plasma periphery has been discussed by Hinton and Ohkawa. Extending their work, the bipolar electron loss is included to obtain the consistent radial electric field. A bifurcation in the particle flux associated with the change of radial electric field is found.

By this mechanism, particle and convective-energy fluxes can have multiple values for the same density/temperature condition near the periphery. This transition occurs in both the limiter and separatrix configurations. The critical edge condition for the transition is obtained.

4) The first model for L-H transition based on E_r change

*1. L- to H- Transition

We study the zero-net-current condition to obtain the radial electric field, E_r. The radial fluxes of the electrons and ions near the plasma periphery (inside the outermost magnetic surface) are calculated. The plasma surface is determined either by the limiter or by the separatrix.

The ion flux in the region of $|a-r| < \rho_p$ is attributed to the direct loss (r: minor radius, a: plasma minor radius, ρ_p: poloidal gyroradius, $v_T m_i qR/aeB_t$, q: safety factor, R: major radius, v_T: thermal velocity of ions, B_t: toroidal magnetic field). The ion loss is given by

$$\Gamma_i^B \sim n_i \rho_p F_i / \sqrt{\varepsilon} \tau_i ,$$

where the coefficient F is proportional to the relative number in the loss cone in the velocity space and $0 < F_i < 1$ ($\varepsilon = r/R$, τ_{ii}^{-1}: ion-ion collision frequency, n_i: ion density). In order to estimate F_i in the presence of E_r, we take two simple assumptions, 1) that the ions which satisfy the resonance condition $v_{//}/qR = E_r/rB$ are lost directly, namely the loss cone shifts in the velocity space, and 2) that the ion distribution function f_i is close to maxwellian, $f_i \propto \exp\{-v_{//}^2/v_T^2\}$. The loss rate scales as

$$F_i = F_i \exp(-\sigma u_E^2),$$

where $u_E = -E_r/(B_p v_T)$, $\sigma = 1$ for the initial L to H transition and $\sigma = 2\varepsilon(1-\cos\theta_m)$ for the case with toroidal rotation due to E_r. Here θ_m simulates the effective poloidal angle of the limiter position.

The electron loss is affected by the microturbulence and can also be bipolar(B). The wave can propagate across the plasma surface to the scrape off layer(SOL) so as to take the electron momentum away. It is also bipolar if it is driven by the magnetic braiding.

$$\Gamma_e^B = -D_e n_e (n_e'/n_e + eE_r/T_e + \alpha T_e'/T_e)$$

where D_e is the anomalous diffusion coefficient and α is a numerical coefficient $\sim O(1)$.

The electric field is determined by the zero-net-current condition, $\Gamma_e^B = \Gamma_i^B$, or

$$\exp(-\sigma X^2) = d(\lambda - X), \qquad (A)$$

where $X = \rho_p e E_r/T_i$, $d = D_e \tau_i \sqrt{\varepsilon}/F_i \rho_p^2$ and $\lambda = -T_e \rho_p (n_e'/n_e + \alpha T_e'/T_e)/T_i$. The convective energy loss associated with Γ^B is given by $Q_{conv}^B = (T_e + T_i)\Gamma$. The total particle flux, Γ_{tot}, is the sum of Γ^B and the intrinsic ambipolar component. The total convective energy loss is given by $Q_{conv}^{tot} = (T_e + T_i)\Gamma_{tot}$.

Figure 1 illustrates the normalized flux $\hat{\Gamma}_{e,i}$ ($\hat{\Gamma}_{e,i} = \Gamma_{e,i}\tau_i \sqrt{\varepsilon}/\hat{F}\rho_p n_i$), as a function of $\rho_p e E_r/T_i$. (The coefficient d may have a weak E_r dependence. We assume that d is independent of E_r.) As is seen from Fig.1, Eq.(A) predicts the transitions of E_r and Γ. When λ is small, Eq.(A) has one

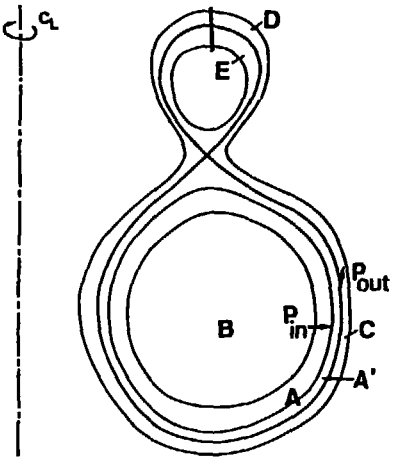

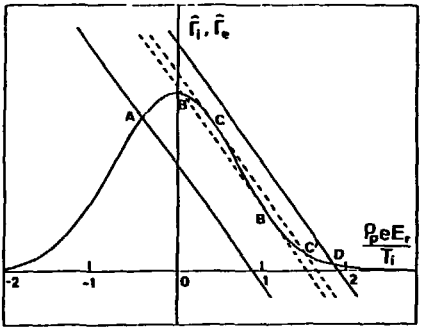

FIG. 1. Fluxes $\hat{\Gamma}_i$, $\hat{\Gamma}_e$ vs the radial electric field. Four cases of λ (with constant d) are shown. Dashed lines indicate the bifurcation condition.

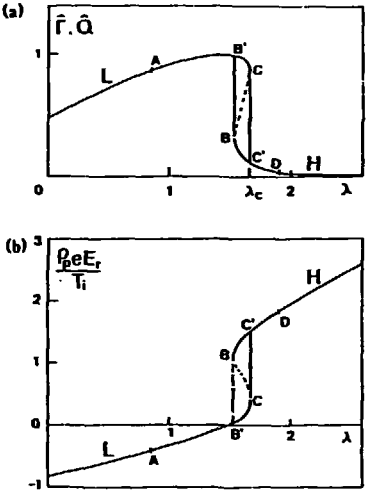

FIG. 2. Solutions for (a) the flux and (b) radial electric field as functions of λ (for the case of $d=1.3$). Points A to D correspond to those in Fig. 1. Transition from the branch of large flux to that of small flux occurs at $\lambda=\lambda_c$.

S.-I. Itoh and K. Itoh, Phys. Rev. Lett. 60, 2276 (1988).

real solution. According to the increase of λ or d, the bifurcation of the solution appears (dotted lines in Fig.1). For the fixed value of d, the transition occurs at the critical value of λ, λ_c.

Figure 2 illustrates the λ dependences of $\hat{\Gamma}$ and $\hat{Q}$ ($\equiv Q_{conv}\tau_{ii}\sqrt{\epsilon}/\hat{F}\rho_p n_i(T_e+T_i)$). There appears a cusp type catastrophe (Riemann-Hugoniot catastrophe). The solutions of Eq.(4) form the cusp-type surface in the space of (λ, d, E_r (or $\hat{\Gamma}$, $\hat{Q}$)). When λ is below the critical value λ_c, the electric field is negative (i.e., directs inward) and the fluxes are large. In the branch of lower fluxes, E_r has an approximate values as $eE_r\rho_p/T_i \simeq \lambda$ ($\lambda > \lambda_c$). The L-mode corresponds to the branch of the large loss flux, and the H-mode is the branch of the reduced loss flux. The transition from the L- to H-mode takes place as A → B' → C → C' → D and that from the H- to L-mode occurs as D → C' → B → B' → A. Because λ_c for the L-to H-mode transition is larger than that for the H- to L-mode transition, there is a hysteresis in the relation of Γ and λ as is shown in Fig.2a. The value λ_c is of the order of unity (about 1.5 in this case). This value is in the range of the experimental observation.

Ambipolar condition is affected by neutrals. Ion momentum is also lost through the charge exchange(CX) process with neutrals. The bifurcation condition is extended to

$$\exp(-\sigma X^2) + d_n(\lambda_i + X) = d(\lambda - X) \qquad (1)$$

where $\lambda_i=-\rho_p(n_i'/n_i+ \alpha_i T_i'/T_i)$, α_i is a coefficient close to 1, $d_n=n_0\tau_i\langle\sigma_{cx}v\rangle\Delta/F_i\rho_p$, Δ is the penetration depth of neutrals given by $v_0/n_e\langle\sigma_{ion}v\rangle$ (v_0: neutral velocity, n_0: neutral particle density).

Figure 1′ shows the bifurcations in Γ and E_r at the criti-

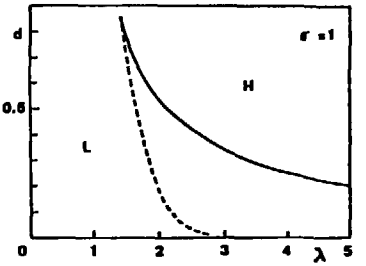

FIG. 2. Criteria for L-to-H-mode (solid line) and H-to-L-mode (dashed line) transition in the d-λ plane ($\sigma = 1$ and $d_n = 0$). Hysteresis appears near the transition condition.

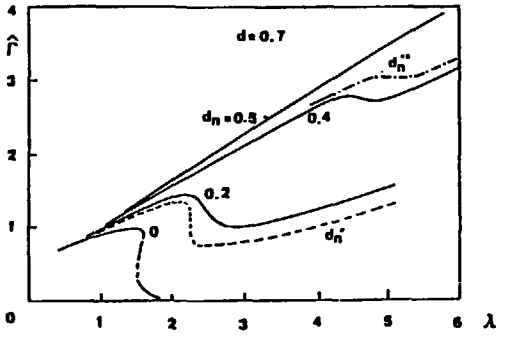

FIG. 6. Normalized flux as a function of the gradient λ in the presence of neutral particles. d_n is chosen as 0, 0.158 (= d_n^*), 0.2, 0.4, 0.429 (= d_n^{**}), and 0.5, respectively. For $d_n > d_n^{**}$, transition is not possible. $\sigma = 1$ and $d = 0.7$.

S.-I. Itoh and K. Itoh, Nucl. Fusion 29, 1031 (1989).

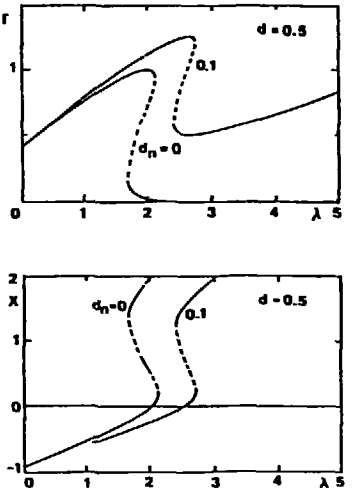

FIG. 1. Normalized flux Γ and radial electric field X as a function of edge gradient λ ($\Gamma = \Gamma_i \sqrt{\epsilon \tau_i / n \rho_p}$, $X = \rho_p e E_r / T_i$). The transition occurs at critical λ, which increases with d_n ($\sigma = 1$, $d = 0.5$).

cal value of λ. The neutrals increase the critical gradient for the transition, and the normalized flux Γ becomes large in the presence of CX loss. The phase diagram of L/H transition on λ-d plane in the presence of neutrals is shown in Fig.2'. The approximate condition is given by $d_\lambda - d_n \lambda_i = 1$. From Fig.2' we see that the condition $\rho_p/\Delta > 1$ is the necessary condition for the transition. From Eq.(1), we have another constraint for existing the bifurcation,(i.e., $\partial\Gamma/\partial\lambda < 0$ for some λ), namely $d_n < \sqrt{e/2\sigma}$.

*2. Transition Condition and Threshold Power

In this model, the threshold value λ_c is predicted. The transition can occur spontaneously. The threshold power for the L- to H-mode transition is interpreted as the necessary power to reach the critical value λ_c. It depends on the confinement nature of the L-mode. The peak value of $\hat{Q}_{conv}$ does not coincide with the threshold power, because there are other losses. Our model predicts that the gradients of the order of ρ_p^{-1} (i.e., the high edge temperature/density) are necessary for the L- to H-mode transition.

The threshold power is obtained as follows. We assume that 1) D_e has the simple form of drift wave turbulence (trapped particles and η_i modes) as $D_e = D_0\sqrt{\varepsilon}MT^{1.5}/B^2Z$, 2) $\nabla n_e/n_e$ is estimated by $-1/\Delta$, 3) $\alpha \simeq \alpha_i \simeq 0$ and $\lambda_i = \lambda \simeq \rho_p/\Delta$. Assumptions 1) and 2) are consistent with the present L-mode scaling of particle confinement time τ_p in JT-60 experiment and a numerical simulation. Taking into account the T-dependences of $\langle\sigma_{ion}v\rangle$ and $\langle\sigma_{cx}v\rangle$ as $\langle\sigma_{ion}v\rangle \simeq 5\times10^{-14}T_h^{\beta}$ m^3/s (T_h is T measured in the unit of 100eV, $\beta > 0$ for T<100eV and $\beta \simeq -1/4$ for T>100eV) and $\langle\sigma_{cx}v\rangle \simeq 10^{-14}T_h^{1/3}$m^3/s, the critical condition is rewritten as

$$25T_h^{5/2+\beta}[1 - 10^3 n_0 B^2 n_e^{-1} B_p^{-1} M^{-1/2} T_h^{-2/3-\beta}] > Z^3 RB^2/MaB_p \quad (2)$$

where we assume $F \sim 1$, $D_0=5m^2/s$ at B=1T and T=100eV, Z is the ionic charge and M is the mass number. For the present day tokamaks, T>100eV is necessary to satisfy inequality(2) and we take $\beta=-1/4$. This fact is also confirmed by a transport code analysis. The power dependence of the edge temperature is obtained from the transport analysis of the scrape-off-layer (SOL). When the classical value of χ and the Bohm-like D are employed, T scales as $T \propto (ZP^2B^2/aI_p n_b)^{2/11}$ where n_b is the boundary density. The power dependence has been confirmed by our numerical simulation of SOL plasmas. If the neutral density is low, the approximate form of the threshold power is given by combining Eq.(2) and T scaling as

$$P_{th} \propto M^{-11/9} Z^{57/18} B^{13/9} I_p^{-13/18} a^{1/2} R^{11/9} n_b^{1/2}. \quad (3)$$

This relation gives favorable dependence on M and I_p and unfavorable dependence on Z, B and machine size. The lower density limit is imposed by the neutrals. From Eq.(2) and the criterion of d_n for bifurcation, we have

$$n_{e_{19}} > 4.2\times10^{-3}\varepsilon^{-2}\, n_{0_{16}} qBM^{-1/2} T_h^{-5/12} \quad (4\text{-}1)$$

$$n_{e_{19}} > (n_{0_{16}} B_p)^{1/2} (\sigma/M)^{1/4} T_h^{19/24} Z^{-1} \quad (4\text{-}2)$$

where n_e, n_0 are given in $10^{19}/m^3$, $10^{16}/m^3$, respectively.

The favorable location of the X-point relative to the ∇B-drift may be explained in relation to the increment of λ and d. Furthermore, the electron edge temperature can be high in the

same configuration, because the distance between the source and sink of the heat flux along the field line is longer compared to the case of the opposite ∇B-drift direction.

According to this model, the transition occurs at the plasma boundary. The improvement of the particle flux is expected and the convective loss to the SOL should be reduced after the transition. Improvement of the particle confinement may further raise the edge temperature, hence the conduction to the SOL may be also reduced due to the collisionless neoclassical effect. The reduction of H_α/D_α radiation is considered to be the result of the reduced convection/conduction losses.

Our model predicts the change of the radial electric field associated with the transition.

The experimental data seems to support the picture that the loss takes two values for one temperature near the edge at the transition condition.

The picture of the multiple flux solution is supported in the observation that the transition is triggered by the small sawtooth.

*3. Temporal Evolution of E_r and Pedestal Formation

After the transition C → C', Γ and $Q_{conv}{}^B$ become about 1/10 times smaller. The loss at the edge, P_{out}, becomes smaller than the flux from the core plasma P_s (= P_{heat}-P_{rad}-P_{cx}). Due to the sudden increase of P_s-P_{out}, the gradients T' and n' start to grow. This occurs in a thin layer near the boundary, $|a-r| < \rho_p$, and gives rise to a formation of the temperature/density pedestal. The conductive and ambipolar components of the loss and the SOL transport determine the steepness of the edge gradient.

When the critical condition is satisfied, the radial

electric field starts to change. The temporal evolution of E_r is governed by the equation

$$(\varepsilon_0\varepsilon_\perp/e)\partial E_r/\partial t = \Gamma_e - \Gamma_i + (\rho_p n_i \mu_\perp / v_{iT})\nabla^2(E_r/B_p) \qquad (5)$$

where $\mu_\perp$ denotes the viscosity. The time scale of E_r change (C→C') is estimated to be $30\sim40\mu s$ for the parameters of R=1.6m, a=0.4m, B=2.5T, q=3, T=0.5keV and $n_e=3\times10^{13}$. Due to the viscosity in Eq.(5), E_r diffuses. The typical time scale is estimated to be 30 ∿ 40 ms for the parameters above, which is of the order of the transport time scale.

*4. Impurity Accumulation, ELM's and H- to L-Mode Transition

The normalized loss flux in the H-branch in Fig.2a is a decreasing function of the gradient. After the transition C → C', a stationary state may not be realized, if there is no other loss. The gradient near the boundary continues to increase until the other losses increase and balance with the heat and particle inputs to the layer.

Due to the steep ion gradient at the edge pedestal, the neoclassical effect causes the inward drift of impurities. We study the H/D plasma in the regime of $Z_I^2 n_I/n_i \sim O(1)$ and $Z_I n_I/n_i \ll 1$. Z_I is the charge of impurity and suffix I denote the impurity. The accumulation modifies the transition condition through the pitch angle scattering and the impurity loss of the losscone. These enhance the bipolar loss of ions. Estimating the width ρ_{pI} as $m_I\rho_p/m_iZ_I$, we have the condition for the positive-E_r branch in the absence of neutrals as, $d\lambda > Z_{eff} + (m_I n_I Z_I/m_i n_i)(F_I/F_i)$.

The critical value, λ_c, is also increased by impurities. Figure 3 illustrates the schematic graph of $E_r(\lambda, n_I/n_i)$ and the trajectory of the parameters. After entering the H-regime

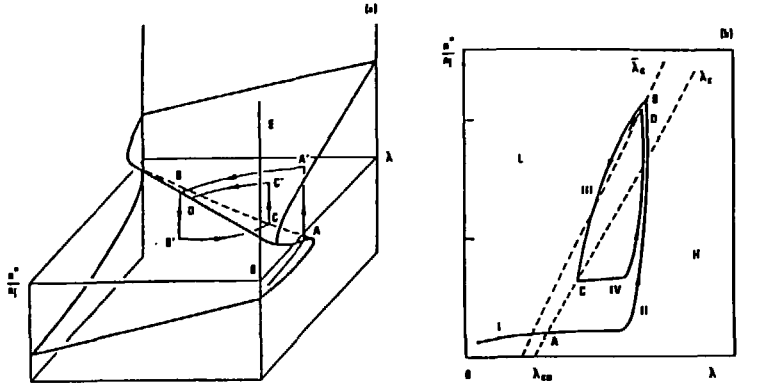

Fig. 3. Schematic drawing of the bistable solution $E_r(\lambda, n^*/n_i)$ and the trajectory of $(\lambda, n^*/n_i, E_r)$ (a). Transitions occur at A, B, C and D (a). The projection on the $(\lambda, n^*/n_i)$ plane is given in (b).

D-III-D

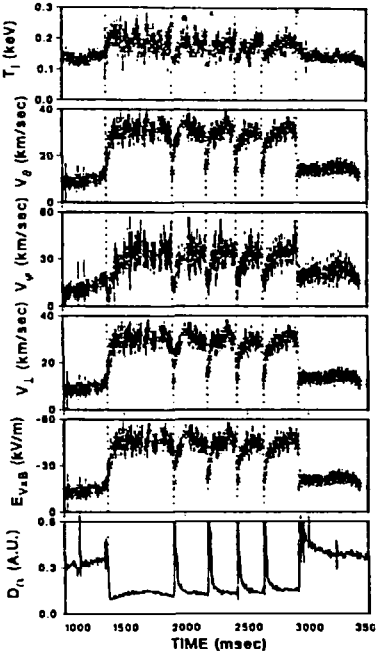

FIG. 4. Change in the edge plasma rotation and the inferred radial electric field at the L to H transition for a neutral beam heated divertor discharge. The D_α trace in the bottom box shows the usual abrupt drop at the time of the L to H transition. The spikes in the D_α signal show the times when several giant edge localized modes (ELM's) occur. Notice that the rotation changes at the transition and then returns momentarily to about the L-mode level at each ELM.

(A→A'), the pedestal grows and the impurity accumulation starts. The diffusion of E_r takes place (A'→B). The impurity accumulation can trigger the transition to the L-phase (B→B'). The pedestal disappears and Z_{eff} reduces (B'→C). Owing to the reduction of Z_{eff}, the plasma recovers to H-mode (C→C'). This short L-phase with a burst would be observed as ELM.

If impurities accumulate in the core plasma so that P_s becomes too small, the recovery to the H-phase is impossible. The reduction of P_s takes place with a time delay (typical value: τ_E). The H-mode can survive after the termination of the additional heating.

*5. Effect on Instabilities near Edge

The effect of E_r on trapped particle instability is examined by calculating the toroidal drift velocity. The change of $J=m\int v_{//}\,d\ell$ and $\tau=\int d\ell/v_{//}$ are calculated from the orbit in the rotating frame, $v_{//}^2= v_{0//}^2-\varepsilon(1-\cos\theta)(v_{0\perp}^2+2v_E^2)+u_g(v_{//}-v_{0//})^2$ where $v_E=v_T u_E$ and u_g is $\rho_p(dE_r/dr)/(v_{iT}B_p)$ corresponding to the effect of dE_r/dr. The toroidal drift is given as $(qR/\tau q_s Br)\partial J/\partial r$ (q_s is the particle charge). Homogeneous E_r causes the same toroidal rotations of electrons and ions (v_E term) and the real frequency shift of the modes, but does not affect the stability. The effect of $\partial E_r/\partial r$ shifts the curvature drift of trapped ions from v_{d0} to $v_{d0}(1+2u_g)$, where $v_{d0}=-mv_{\perp 0}^2 qR/2q_sBr^2$. If $\partial E_r/\partial r$ is negative and $\partial/\partial r$ is estimated by the banana size $\sim\sqrt{\varepsilon}/\rho_p$, the toroidal drift velocity of trapped electrons reduces by the factor of $1-2\sqrt{\varepsilon}$. The growth rates of trapped particle instabilities are reduced.

In order to conclude the effect on the stability, the combined analysis on transport of the plasma and electric field and the stability is necessary.

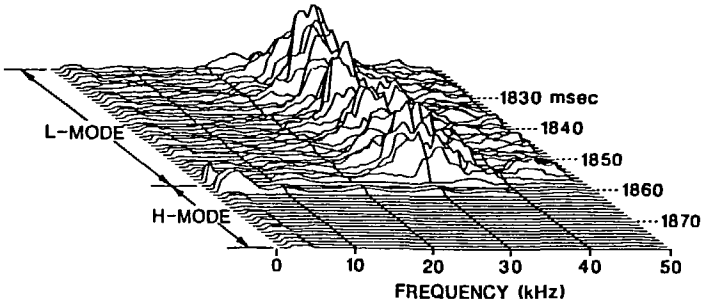

Fig. 1. Plot of auto power spectrum of magnetic fluctuations at various times in a divertor discharge. Note decrease of fluctuations in the 10–30 kHz range at the L to H transition. The signal shown here comes from a magnetic probe under the divertor tiles near the point where the outer separatrix intersects the tiles. The 3 db point of the frequency response of these probes is 50 kHz.

H-mode discharges in DIII-D

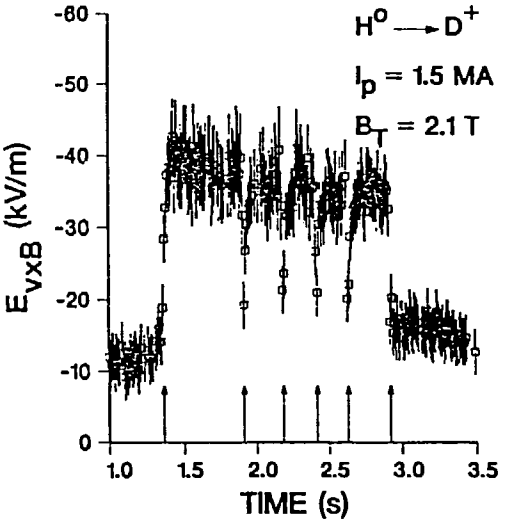

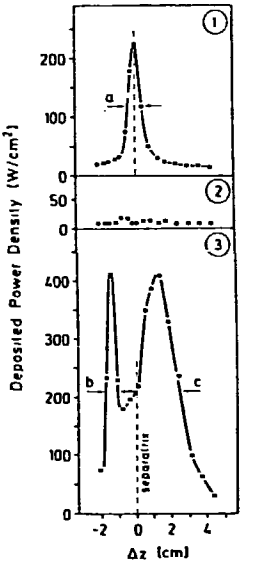

Fig. 3. Contribution to the edge radial electric field from plasma rotation as a function of time across the L to H transition. The first arrow on the X-axis indicates the time of the L to H transition. The next four arrows show when ELMs occur. The final arrow indicates the H to L transition. Notice that the electric field returns almost to its L-mode value during an ELM event. Time resolution of the spectroscopic system is 10 ms for these data.

K. H. Burrell *et al.*, Plasma Phys. Controlled Nucl. Fusion **31**, 1649 (1989).

Difficulties found in our model theory and re-modelling

--- Critical comments from ASDEX and D-III-D and other works

The possible influence of electric fields on the L-H transition was first pointed out in this model.... At least in a qualitative sense, this L-H transition model reproduces many experimental observations very well.

*In fact, we observe a reduction of the power flux in the separatrix and a loss of power accountability....

--- (convective loss vs conductive loss)

*This model identifies the good confinement branch as the branch having positive electric field.... However, recent measurements of the poloidal rotation of the plasma in the separatrix region of D-III-D also give results which are in contrast to those predicted by the model...

--- ($E_r > 0$ or $E_r < 0$)

*In this model, no change of the turbulent fluctuation level are required for better confinement, contrary to experimental observations. Experiments in D-III-D have revealed and confirmed the statements above. (see figures)

<Re-modelling>

The H-mode transition models based on the sudden change of E_r have been reported, and the change in edge E_r have been observed in experiments. However, neither of models could fully explain the H-mode transition. We extend our previous theory, including the effects of E_r'. Ion losscone rate changes in the presence of E_r'; banana width and the minimum energy which bounds the loss cone region alter. Introducing u_g, $(=\rho_p E_r'/v_{Ti}B_p)$ and numerics F and C, we have

$$\Gamma_{i,B}=(Fn_i\nu_i\rho_p/\sqrt{\varepsilon}\sqrt{|1-u_g|+C\varepsilon})\exp\{-\sigma|1-u_g|X^2\},\ X=\rho_p eE_r/T_i$$

where $\varepsilon=a/R$ (a,R; minor, major radius) and σ indicates limiter place.

Electron flux is assumed to be anomalous due to drift-type microturbulence of toroidal mode number N. Applying the mixing length theory,

$$\Gamma_{s,a} = -D_s n_s[\frac{n_s'}{n_s}(1+\alpha_s\eta_s) -\beta_s(\frac{eE_r}{T_s} -\frac{eqR_\omega B_t}{NcT_s})] \qquad (1)$$

where $D_e=D_{e0}\sqrt{1+u_g/u_c}$, $u_c^2=8\sqrt{2\varepsilon}(4-u_c)$, $\eta=d\ln T/d(\ln n)$, q and β denote safety factor and the coefficient of anomalous electron viscosity. Note that the shear term of E_r/r in Eq.(1), (differential rotation affects the particle flux. $\Gamma_{e,a}=\Gamma_{i,B}$ gives the refined condition for transition. Transition (L-H) occurs even in the case of $\sigma=0$ (limiter case), associated with the negative jump of E_r', independent of the sign of E_r. Sudden reductions of fluctuations and conduction loss are predicted. Critical gradient, λ_c, of new model is close to the value obtained from previous model in the presence of toroidal rotation, $U_\phi=(qT_iR/erB)[n_i'/n_i(1+c_i\eta_i)-eE_r/T_i]$.

At present, there are still arguments about the onset of L - H transition and we do not fully understand the physics.....

Another model theory based on the bifurcation of the poloidal flow is also a plausible candidate to explain the H mode transition. (K.C. Shaing and E.C.Crume,Jr., PRL 63 2369 (1989))

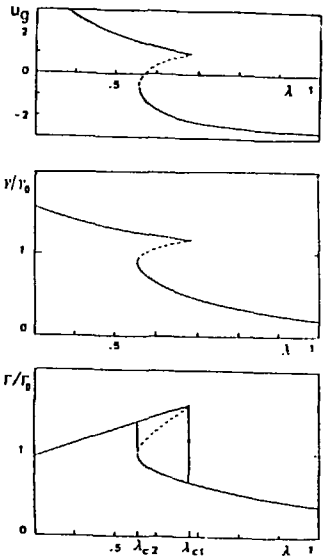

Fig. 1. Gradient of E_r, instability growth rate γ, and particle flux as a function of the gradient parameter λ. Multiple solutions simultaneously exist for λ, and transition takes place at a particular value of λ. Parameters are $d=0.5$, $u_c=2.76$, $C=2$ and $\varepsilon=0.3$. Normalized value Γ_0 is given as $Fn_i\nu_i\rho_p/2\sqrt{\varepsilon}$.

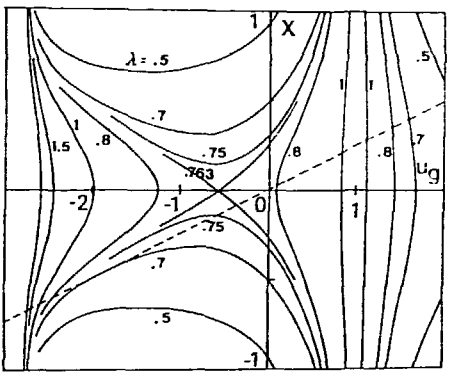

The solution of Eq.(4) on u_g-X plane is drawn for various values of λ. The dashed line corresponds to $E_r=\eta E_r' p_p$. Depending on the coefficient η, the appearance of the transition slightly changes. Parameters are d=1.0, σ=0.5, u_c=3.0, C=2.0 and ε=0.3.

Edge Electric-Field Profiles of *H*-Mode Plasmas in the JFT-2M Tokamak

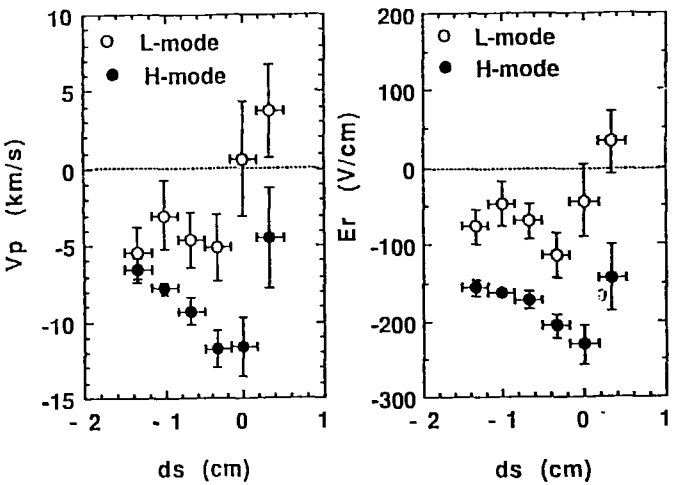

Lecture 3

-- ELMy-H mode as Limit Cycle and Chaotic Oscillations in Tokamak Plasmas

The ELMs have shown a variety of appearances and appear in a some restricted parameter space of the H phase. They are the single ELM, big/small ELMs or grassy ELMs associated with a quasi-periodic oscillation of H_α bursts, and their mixtures. Their phenomenological characterization has recently been begun in experiments. The H-mode with small and frequent ELMs is a candidate for standard operation in future experimental tokamak reactor. However, key physical mechanisms for discriminating various kinds of ELMs are not yet known.

Giant-ELMs and small-ELMs have a similar ratio between the period of the ELM and the duration of each burst, which is of the order of 10. In grassy-ELMs, a different type of oscillation has been observed. The period and duration of the burst have similar values as is shown in Fig.1. Grassy ELMs, which we analyse, only appear near the L/H transition boundary.

A comparison with critical-β analysis due to the MHD ballooning mode has been applied. The analyses have shown that the onset of some ELMs occurs far below the critical pressure gradient. Resistive MHD analysis of a surface peeling mode may partly explain ELMs. However, there remains a question for MHD models why the structure of fluctuation/transport is insensitive to the surface q value and current profile. The period and duration of the grassy ELMs are left unsolved in MHD analysis.

A model of ELM as a cyclic oscillation between L and H phases due to impurity accumulation has been proposed. Up to now, however, the impurity accumulation is considered to be

the associated phenomena.

We here propose a more complete model of grassy-ELMs (p.51 Fig.1). The L/H transition has been observed to have a hysteresis curve between the thermodynamic forces and associated flows. Theories have predicted the sudden L/H transition associated with the radial electric field change and they are extended to include the temporal evolution and the spatial diffusion. The obtained equations for the edge density and the radial electric field are of the time-dependent Ginzburg-Landau type, which contains the solution of a limit cycle oscillation. This oscillation is attributed to be one class of grassy-ELMs. A model S-curve is employed in the phase diagram of the density gradient and the particle flux. The internal structure is obtained and shows the existence of an intermediate state (mesophase) of L and H phases near the edge region. We assume a uniform temperature, since the ELMs discussed in this paper are experimentally insensitive to the heating power.

Model equations consist of the radial transport equations for the density n with the effective diffusivity D, and for the normalized radial electric field (or poloidal rotation) Z with the viscous diffusivity μ. The value of D can be multi-valued and is a function of Z. The equations contain a force, which is a nonlinear function of the density gradient and are given by

$$\frac{\partial n}{\partial t} = \frac{\partial}{\partial x} D(Z) \frac{\partial n}{\partial x} \qquad (1)$$

$$\varepsilon \frac{\partial Z}{\partial t} = -N(Z;g) + \mu \frac{\partial^2 Z}{\partial x^2} \qquad (2)$$

The nonlinear operator N is proportional to the radial current $\Gamma_e-\Gamma_i$, which arises from ion orbit loss, drift wave convection and ion parallel viscous damping. Solutions Z(g) in L and H phases are given by N(Z;g) =0 ($g \propto \rho_p n'/\nu n$; ρ_p is the ion poloidal gyroradius and ν is the ion collisionality.), which show the transition between multiple states. The parameter ε indicates a small coefficient showing that Eq.(2) has a faster time scale than Eq.(1) when μ and D have similar magnitude. The curve of N(Z,g)=0 for the given value of g_0 is shown in Fig.2. The large D and the small D branches correspond to the L and the H states, respectively. In the zero-dimensional analysis, the transition from L to H or H to L occurs at certain values of g (A→B [L→H] or B'→A' [H→L]). The radial and temporal structure Z(x,t) is obtained here.

To model the dynamics of the L/H transition, we use the simple S-curve of N and D as

$$N(Z,g) = g-g_0+[\beta Z^3-\alpha Z]$$

$$D(Z) = (D_{max}+D_{min})/2 + [(D_{max}-D_{min})/2]\cdot\tanh Z$$

In writing explicit forms of N and D, we normalize x in ρ_p, D and μ in D_0 (which are typical values in the L-phase), t in $\rho_p{}^2/D_0$, and flux Γ in $D_0 n_0/\rho_p$. The normalizing density n_0 is chosen so as to satisfy g_0=1. $\varepsilon \simeq (\rho/\rho_p)^2$ (ρ is the ion gyroradius). In the following, we use the normalized variables. μ/D_0 is the diffusion Prandtl number P_D. Parameters g_0, α, β, D_{max}, D_{min} and μ/D_0 are treated as constant.

We numerically solve Eqs.(1) and (2) assuming that $\varepsilon \ll 1$. Actually, we here take a simple condition that $\partial Z/\partial t = 0$ (ε = 0) to solve the temporal evolution of the density. Equation (2) is a kind of time dependent Ginzburg-Landau equation or

the one which is used to analyse the reaction diffusion system in chemical reactions. The system contains so-called slow manifold structure due to the assumption with respect to the time scales.

The slab region near the plasma edge, $-L<x<0$, is our interest. As the boundary conditions, at the plasma edge ($x=0$), we impose the constraint that $(n'/n)^a n^b$ is fixed. We discuss the case of $a=1$ and $b=0$. At the core side ($x=-L$), we give the particle flux Γ_{in}.

Solving Eqs.(1) and (2) with $\varepsilon=0$ we find the state with the periodic oscillations of the edge density n_s and the loss flux Γ_{out} in the restricted parameter space near the boundary of the L and H phases. The flux Γ_{out} is defined at $x=0$. In Fig.3, the temporal evolutions of Γ_{out} (a), which corresponds to the H_α burst, and the Lissajous figure of n_s and Γ_{out} (b) are shown. The parameters are; $g_0=1$, $\alpha=0.2$, $\beta=0.2$, $D_{max}=3$, $D_{min}=0.1$, $\mu=1$, $\Gamma_{in} = 1.25$ and $\lambda_s(\equiv -n/n'$ at the edge$)= 1$.

These oscillating solutions are possible in the intermediate regime between L and H phases, and are attributed to ELMy-H mode. The time averaged density is between that in L phase and that in H phase. The parameter space where the ELMy-H mode appears is found to be

$$D_m/(g_m\lambda_s) < \Gamma_{in}\lambda_s < D_M/(g_M\lambda_s), \qquad (3)$$

where $g_m= g_0-2\beta(\alpha/3\beta)^{3/2}$, $g_M= g_0+2\beta(\alpha/3\beta)^{3/2}$, $D_m=D(Z=\sqrt{\alpha/3\beta})$ and $D_M=D(Z=-\sqrt{\alpha/3\beta})$ and $\lambda_s \propto g^{-1}$, as shown in Fig.2. In this parameter regime, the cross-over point of the hysteresis curve and the g value at the edge becomes unstable and the limit cycle solution on the g and D plane (see Fig.2) appears. When Γ_{in} is large so as to satisfy $\Gamma_{in}\lambda_s^2 > D_M/g_M$ we find the stationary L state ; and the H state with steep density grad-

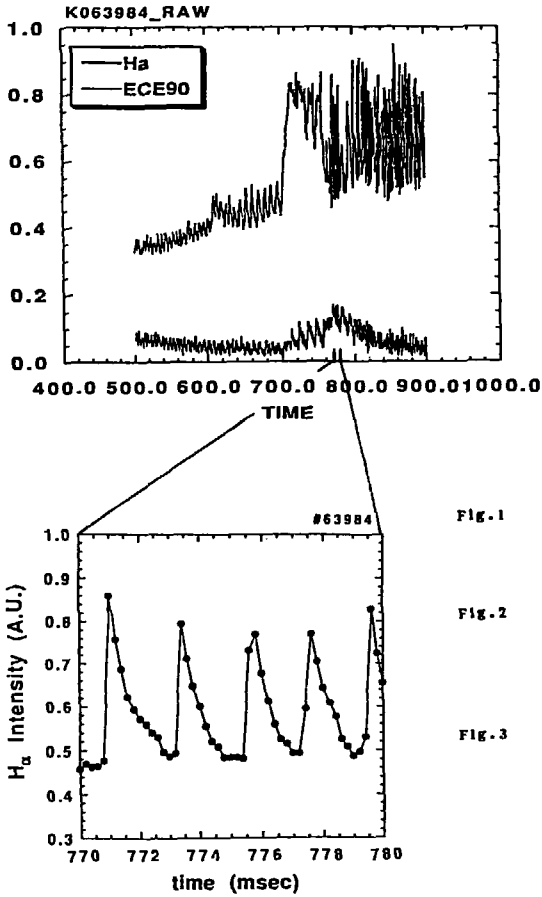

Fig. 1

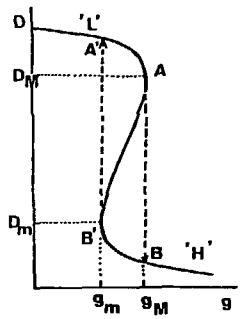

Fig.2

Fig.1 Time trace of the H_α intensity of the grassy H-mode in the JFT-2M tokamak. H_α is given in arbitrary units. For details of the discharge conditions, see Ref

Fig.2 Model of effective diffusivity D (i.e., ratio of the particle flux to the density gradient) as a function of gradient parameter g. See text for the definition and normalization. (α=1, g=1, D_{max}=3, D_{min}=0.1, g_0=1).

Fig.3 Temporal evolution of the outflux(a) and the Lissajous figure between the edge density and the outflux(b). Parameters are μ=1, Γ_{in}=1, λ_s=1.25, and others are the same as in Fig.2. Spatial profiles of density (c) and diffusivity (d). Time slice is denoted by arrows in (a). Solid and dashed lines show before the burst and end of the burst, respectively.

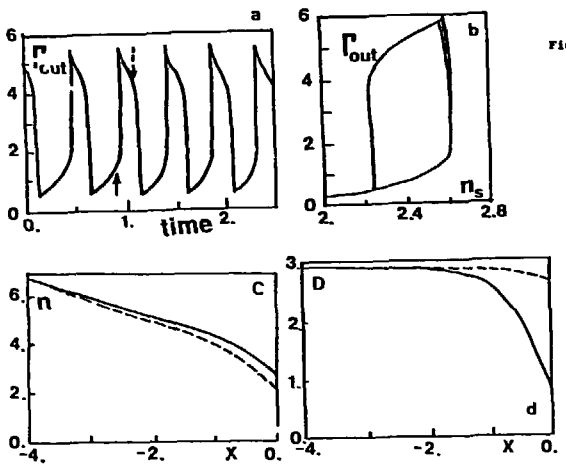

Fig.3

ient is found in the region $\Gamma_{in}\lambda_s^2 < D_m/g_m$. Therefore the ELMy-H state found here is the mesophase of L and H phases. If the condition $D_m/g_m > D_M/g_M$ holds, no oscillation is allowed.

The existence of the mesophase of the L and H phases is seen in the radial structure of the density and the effective diffusion coefficient D. In Fig.3 (c) and (d), their radial structures are shown at the times of high and the low confinement. A transport barrier is formed in a phase of rising density. A smooth curve of D is formed due to the finite viscosity μ. The thickness of the barrier, Δ, is estimated as $\Delta \simeq \sqrt{2\beta\mu/\alpha}$ in the small μ limit. Numerical calculation gives $\Delta \propto \mu^{0.44}$, confirming this analysis. (L satisfies $L \gg \Delta$, so that Δ is not limited by the computation region.) In this region, there exists the poloidal rotation. The radial width Δ is different from the width of the density inversion region.

We study the parameter dependence of the period τ of the oscillation. The numerical computation gives $\tau \simeq C\alpha\lambda_s\Delta D_M^{-1}$ where C is a numerical coefficient of the order of unity. As is shown in Eq.(3), λ_s is bounded in a narrow region to realize the oscillation. If the ratio λ_s^2/D_M and other parameters are fixed, we have $\tau \propto D_M^{-0.5}$ over a wide range. On the other hand, if the value of $\Gamma_{in}\lambda_s^2$ and other parameters are fixed, we have $\tau \propto \Gamma_{in}^{-0.5}$.

The ratio of the time interval of good confinement (τ_H) to τ, $\eta = \tau_H/\tau$, represents how close the intermediate state is to the H-mode. (In the H-mode, $\eta=1$; $\eta=0$ for the L-mode). In the parameter space predicted by Eq.(3), η takes intermediate values between one and zero. η is a decreasing function of $\Gamma_{in}\lambda_s^2$, and is discontinuous at the boundaries D_m/g_m and D_M/g_M. For oscillating solutions, η takes its largest value η_{max} at $\Gamma_{in}\lambda_s^2 = D_m/g_m$. η_{max} increases and approaches unity if D_m becomes close to D_{min}. This is confirmed by reducing D_m to

D_{min} by fixing g_m. For instance, by taking α=0.2 and $\beta=\alpha^3$, η can be greater than 0.95, i.e., the period is 20 times longer than the pulse width. In other words, the H-ness depends on the transition structure.

This model with ε=0 produces the periodic birth and decay of the transport barrier and associated bursts of the outflux from the plasma surface. For the case of $\varepsilon \neq 0$, another time scale is introduced in the solutions of Eq.(1) and (2). Chaotic as well as intermittent appearances of the bursts are predicted. When we introduce the neutral particle effect to Eq.(1) as a random noise, we also observe the intermittent state and the chaotic appearances depending on its noise level.

In summary, the theoretical model of ELMs are developed by extending the bifurcation model to the time-dependent diffusive media. A time-dependent Ginzburg-Landau model equation with the spatial diffusion is applied. A periodic solution of the plasma density and outflux is found revealing a sequence of bursts of plasma loss. The mesophase is found near the plasma boundary. The width of the transport barrier was found to be proportional to $\sqrt{P_D}$. This model reproduces the oscillations in which the decay time of the loss and period are comparable. The region of this nonlinear oscillation is identified in the parameter space; oscillations appear near the H/L mode boundary. These features are consistent with experimental observations of the grassy-ELMs. The parameter dependences of the period and "H-ness" η are studied to identify the intermediate state. The finite diffusion time of the electric field leads to chaotic oscillations. Fluctuations in the source flux or external oscillations also cause additional chaotic oscillations of n, Γ_{out} and E_r.

Acknowledgement

The author expresses her heartily thank to Dr. K. Itoh for his continuous encouragement as well as for scientific advices. She also acknowledges elucidating discussions with Drs. F. Wagner, K. Lackner, F. L. Hinton, T. Ohkawa, S. Tsuji, K. Ida, Y. Miura, K. C. Shaing, members of the ASDEX group and the JFT-2M group. She wishes to thank Dr. A. Fukuyama for continuous discussions and the collaborations. This work is partly supported by the Grant-in-Aid for Fusion Research of MOE Japan.

References for Lectures 1, 2 & 3

[1] F. Wagner, G. Becker, K. Behringer, et al., Phys. Rev. Lett. **49** (1982) 1408.

[2] F. Wagner, G. Fussmann, G. Grave, et al., Phys. Rev. Lett. **53** (1984) 1453.

[3] M. Keilhacker, G. Becker, K. Bernhardi, et al., Plasma Phys. Controlled Fusion **26** (1984) 49.

[4] F. Wagner, M. Keilhacker, et al., J. Nucl. Mater. **121** (1984) 103.

[5] E. R. Muller et al., J. Nucl. Mater. **121** (1984) 138.

[6] F. Wagner, K. Lackner, in *Physics of the Plasma Wall Interactions in Controlled Fusion* (ed. D. E. Post and H. Behrisch, NATO ASI Series **B131**, Prenum Press, 1984) 931.

[7] M. Keilhacker, G. v. Gierke, E. R. Muller, et al., Plasma Phys. Controlled Fusion **28** (1986) 29.

[8] T. Ohkawa, F. L. Hinton, *Plasma Physics and Controlled Nuclear Fusion Research 1986* (Proc. 11th Int. Conf. Kyoto 1986) Vol.2, IAEA, Vienna (1987) 221.

[9] S. Tsuji, and JT-60 Team, in *Proceedings of 14th European Conference on Controlled Fusion and Plasma Physics* (Madrid, 1987) Vol.1, 57.

[10] S.-I. Itoh, K. Itoh, Phys. Rev. Lett. **60** (1988) 2276.

[11] K. Itoh and S.-I. Itoh, Plasma Phys. Controlled Fusion **31** (1989) 487.

[12] S.-I. Itoh and K. Itoh, Nucl. Fusion **29** (1989) 1031.

[13] T. Ohkawa, S.-I. Itoh, K. Itoh, Kakuyugo Kenkyu, **59** (1988) 488.

[14] K. C. Shaing, W.A. Houlberg, E.C. Crume, Comments Plasma Phys. Controlled Fusion **12** (1988) 69.

[15] K. Shimizu, T. Hirayama, H. Shirai, et al., J. Nucl. Mater. **162-164** (1989)

[16] K. C. Shaing, E. C. Crume, Phys. Rev. Lett. **63** (1989) 2369.

[17] R. J. Taylor, M. L. Brown, B. D. Fried, H. Grote, J. R. Liberati, G. J. Morales, P. Pribyl, D. Darrow, M. Ono, Phys. Rev. Lett. **63** (1989) 2365.

[18] The ASDEX Team, Nucl. Fusion **29** (1989) 1959, and the papers cited there in.

[19] P. Gohil, M.A. Mardavi, L. Lao, et al., Phys, Rev. Lett. **61** (1988) 1603 ; D.H. Hill, T. Petrie, M.A. Mardavi, et al., Nucl. Fusion **28** (1988) 902 ; D.P. Schissel, K.H. Burrell, J.C. DeBoo, et al., Nucl. Fusion **29** (1989) 185.

[20] K. H. Burrell, et al., Plasma Phys. Controlled Fusion **31** (1989) 1649.

[21] DIII-D Team, in *Plasma Physics and Controlled Nuclear Fusion Research, 1990,* Proceedings of the 13th International Conference, Washington USA, paper CN-53/A-1-4.

[22] JT-60/JFT-2M joint meeting, (1990) JAERI-memo 01-478.

[23] T. Shoji, et al., in *Controlled Fusion and Plasma Physics (Proc. 17th Eur.Conf.Amsterdam,1990)*, Part 3 (1990) 1452.

[24] Y. Miura, H. Aikawa, K. Hoshino, et al., in *Plasma Physics and Controlled Nuclear Fusion Research, 1990,* Proceedings of the 13th International Conference, Washington USA, paper CN-53/A-4-6.

[25] T. Osborne, K.H. Burrell, T. Carlstrom, et al., Bull. Am. Phys. Soc. **35** (1990) 1975.

[26] F. Wagner, F. Ryter, A.R. Field, et al., in *Plasma Physics and Controlled Nuclear Fusion Research, 1990,* Proceedings of the 13th International Conference, Washington USA, paper CN-53/A-4-2.

[27] R. J. Groebner, K. H. Burrell, R. P. Seraydarian, Phys. Rev. Lett. **64** (1990) 3015.

[28] K. Ida, S. Hidekuma, Y. Miura, T. Fujita, M. Mori, K. Hoshino, N. Suzuki, T. Yamauchi, JFT-2M Group,, Phys. Rev. Lett. **65** (1990) 1364.

[29] S.-I. Itoh and K. Itoh, J. Phys. Soc. Japan **59** (1990) 3815.

[30] S.-I. Itoh, K. Itoh, A. Fukuyama, Y. Miura & JFT-2M gr., NIFS rep.#87 (National Institute for Fusion Science).

Recent Issues of NIFS Series

NIFS-40 K. Toi, Y. Hamada, K. Kawahata, T. Watari, A. Ando, K. Ida, S. Morita, R. Kumazawa, Y. Oka, K. Masai, M. Sakamoto, K. Adati, R. Akiyama, S. Hidekuma, S. Hirokura, O. Kaneko, A. Karita, T. Kawamoto, Y. Kawasumi, M. Kojima, T. Kuroda, K. Narihara, Y. Ogawa, K. Ohkubo, S. Okajima, T. Ozaki, M. Sasao, K. Sato, K.N. Sato, T. Seki, F. Shimpo, H. Takahashi, S. Tanahashi, Y. Taniguchi and T. Tsuzuki, *Study of Limiter H- and IOC- Modes by Control of Edge Magnetic Shear and Gas Puffing in the JIPP T-IIU Tokamak*; Sep. 1990

NIFS-41 K. Ida, K. Itoh, S.-I. Itoh, S. Hidekuma and JIPP T-IIU & CHS Group, *Comparison of Toroidal/Poloidal Rotation in CHS Heliotron/Torsatron and JIPP T-IIU Tokamak*; Sep .1990

NIFS-42 T.Watari, R.Kumazawa,T.Seki, A.Ando,Y.Oka, O.Kaneko, K.Adati, R.Ando, T.Aoki, R.Akiyama, Y.Hamada, S.Hidekuma, S.Hirokura, E.Kako, A.Karita, K.Kawahata, T.Kawamoto, Y.Kawasumi, S.Kitagawa, Y.Kitoh, M.Kojima, T. Kuroda, K.Masai, S.Morita, K.Narihara, Y.Ogawa, K.Ohkubo, S.Okajima, T.Ozaki, M.Sakamoto, M.Sasao, K.Sato, K.N.Sato, F.Shinbo, H.Takahashi, S.Tanahashi, Y.Taniguchi, K.Toi, T.Tsuzuki, Y.Takase, K.Yoshioka, S.Kinoshita, M.Abe, H.Fukumoto, K.Takeuchi, T.Okazaki and M.Ohtuka, *Application of Intermediate Frequency Range Fast Wave to JIPP T-IIU and HT-2 Plasma*; Sep. 1990

NIFS-43 K.Yamazaki, N.Ohyabu, M.Okamoto, T.Amano, J.Todoroki, Y.Ogawa, N.Nakajima, H.Akao, M.Asao, J.Fujita, Y.Hamada, T.Hayashi, T.Kamimura, H.Kaneko, T.Kuroda, S.Morimoto, N.Noda, T.Obiki, H.Sanuki, T.Sato, T.Satow, M.Wakatani, T.Watanabe, J.Yamamoto, O.Motojima, M.Fujiwara, A.Iiyoshi and LHD Design Group, *Physics Studies on Helical Confinement Configurations with l=2 Continuous Coil Systems*; Sep. 1990

NIFS-44 T.Hayashi, A.Takei, N.Ohyabu, T.Sato, M.Wakatani, H.Sugama, M.Yagi, K.Watanabe, B.G.Hong and W.Horton, *Equilibrium Beta Limit and Anomalous Transport Studies of Helical Systems*; Sep. 1990

NIFS-45 R.Horiuchi, T.Sato, and M.Tanaka, *Three-Dimensional Particle Simulation Study on Stabilization of the FRC Tilting Instability*; Sep. 1990

NIFS-46 K.Kusano, T.Tamano and T. Sato, *Simulation Study of Nonlinear Dynamics in Reversed-Field Pinch Configuration*; Sep. 1990

NIFS-47 Yoshi H.Ichikawa, *Solitons and Chaos in Plasma*; Sep. 1990

NIFS-48 T.Seki, R.Kumazawa, Y.Takase, A.Fukuyama, T.Watari, A.Ando, Y.Oka, O.Kaneko, K.Adati, R.Akiyama, R.Ando, T.Aoki, Y.Hamada, S.Hidekuma, S.Hirokura, K.Ida, K.Itoh, S.-I.Itoh, E.Kako, A. Karita, K.Kawahata,

T.Kawamoto, Y.Kawasumi, S.Kitagawa, Y.Kitoh, M.Kojima, T.Kuroda, K.Masai, S.Morita, K.Narihara, Y.Ogawa, K.Ohkubo, S.Okajima, T.Ozaki, M.Sakamoto, M.Sasao, K.Sato, K.N.Sato, F.Shinbo, H.Takahashi, S.Tanahashi, Y.Taniguchi, K.Toi and T.Tsuzuki, *Application of Intermediate Frequency Range Fast Wave to JIPP T-IIU Plasma*; Sep.1990

NIFS-49 A.Kageyama, K.Watanabe and T.Sato, *Global Simulation of the Magnetosphere with a Long Tail: The Formation and Ejection of Plasmoids*; Sep.1990

NIFS-50 S.Koide, *3-Dimensional Simulation of Dynamo Effect of Reversed Field Pinch*; Sep. 1990

NIFS-51 O.Motojima, K. Akaishi, M.Asao, K.Fujii, J.Fujita, T.Hino, Y.Hamada, H.Kaneko, S.Kitagawa, Y.Kubota, T.Kuroda, T.Mito, S.Morimoto, N.Noda, Y.Ogawa, I.Ohtake, N.Ohyabu, A.Sagara, T. Satow, K.Takahata, M.Takeo, S.Tanahashi, T.Tsuzuki, S.Yamada, J.Yamamoto, K.Yamazaki, N.Yanagi, H.Yonezu, M.Fujiwara, A.Iiyoshi and LHD Design Group, *Engineering Design Study of Superconducting Large Helical Device*; Sep. 1990

NIFS-52 T.Sato, R.Horiuchi, K. Watanabe, T. Hayashi and K.Kusano, *Self-Organizing Magnetohydrodynamic Plasma*; Sep. 1990

NIFS-53 M.Okamoto and N.Nakajima, *Bootstrap Currents in Stellarators and Tokamaks*; Sep. 1990

NIFS-54 K.Itoh and S.-I.Itoh, *Peaked-Density Profile Mode and Improved Confinement in Helical Systems*; Oct. 1990

NIFS-55 Y.Ueda, T.Enomoto and H.B.Stewart, *Chaotic Transients and Fractal Structures Governing Coupled Swing Dynamics*; Oct. 1990

NIFS-56 H.B.Stewart and Y.Ueda, *Catastrophes with Indeterminate Outcome*; Oct. 1990

NIFS-57 S.-I.Itoh, H.Maeda and Y.Miura, *Improved Modes and the Evaluation of Confinement Improvement*; Oct. 1990

NIFS-58 H.Maeda and S.-I.Itoh, *The Significance of Medium- or Small-size Devices in Fusion Research*; Oct. 1990

NIFS-59 A.Fukuyama, S.-I.Itoh, K.Itoh, K.Hamamatsu, V.S.Chan, S.C.Chiu, R.L.Miller and T.Ohkawa, *Nonresonant Current Drive by RF Helicity Injection*; Oct. 1990

NIFS-60 K.Ida, H.Yamada, H.Iguchi, S.Hidekuma, H.Sanuki, K.Yamazaki and CHS Group, *Electric Field Profile of CHS Heliotron/Torsatron Plasma with Tangential Neutral Beam Injection*; Oct. 1990

NIFS-61 T.Yabe and H.Hoshino, *Two- and Three-Dimensional Behavior of Rayleigh-Taylor and Kelvin-Helmholz Instabilities*; Oct. 1990

NIFS-62 H.B. Stewart, *Application of Fixed Point Theory to Chaotic Attractors of Forced Oscillators;* Nov. 1990

NIFS-63 K.Konn., M.Mituhashi, Yoshi H.Ichikawa,*Soliton on Thin Vortex Filament;* Dec. 1990

NIFS-64 K.Itoh, S.-I.Itoh and A.Fukuyama,*Impact of Improved Confinement on Fusion Research;* Dec. 1990

NIFS -65 A.Fukuyama, S.-I.Itoh and K. Itoh,*A Consistency Analysis on the Tokamak Reactor Plasmas;* Dec. 1990

NIFS-66 K.Itoh, H. Sanuki, S.-I. Itoh and K. Tani,*Effect of Radial Electric Field on α-Particle Loss in Tokamaks;* Dec. 1990

NIFS-67 K.Sato,and F.Miyawaki,*Effects of a Nonuniform Open Magnetic Field on the Plasma Presheath*; Jan.1991

NIFS-68 K.Itoh and S.-I.Itoh,*On Relation between Local Transport Coefficient and Global Confinement Scaling Law;* Jan. 1991

NIFS-69 T.Kato, K.Masai, T.Fujimoto,F.Koike, E.Källne, E.S.Marmar and J.E.Rice,*He-like Spectra Through Charge Exchange Processes in Tokamak Plasmas;* Jan.1991

N'FS-70 K. Ida, H. Yamada, H. Iguchi, K. Itoh and CHS Group, *Observation of Parallel Viscosity in the CHS Heliotron/Torsatron* ; Jan.1991

NIFS-71 H. Kaneko, *Spectral Analysis of the Heliotron Field with the Toroidal Harmonic Function in a Study of the Structure of Built-in Divertor* ; Jan. 1991

NIFS-72 S. -I. Itoh, H. Sanuki and K. Itoh, *Effect of Electric Field Inhomogeneities on Drift Wave Instabilities and Anomalous Transport* ; Jan. 1991

NIFS-73 Y.Nomura, Yoshi.H.Ichikawa and W.Horton, *Stabilities of Regular Motion in the Relativistic Standard Map*; Feb. 1991

NIFS-74 T.Yamagishi, *Electrostatic Drift Mode in Toroidal Plasma with Minority Energetic Particles*, Feb. 1991

NIFS-75 T.Yamagishi, *Effect of Energetic Particle Distribution on Bounce Resonance Excitation of the Ideal Ballooning Mode*, Feb. 1991

NIFS-76 T.Hayashi, A.Tadei, N.Ohyabu and T.Sato, *Suppression of Magnetic Surface Breading by Simple Extra Coils in Finite Beta Equilibrium of Helical System;* Feb. 1991

NIFS-77 N. Ohyabu, *High Temperature Divertor Plasma Operation*; Feb. 1991

NIFS-78 K.Kusano, T. Tamano and T. Sato, *Simulation Study of Toroidal Phase-Locking Mechanism in Reversed-Field Pinch Plasma*; Feb. 1991

NIFS-79 K. Nagasaki, K. Itoh and S. -I. Itoh, *Model of Divertor Biasing and Control of Scrape-off Layer and Divertor Plasmas*; Feb. 1991

NIFS-80 K. Nagasaki and K. Itoh, *Decay Process of a Magnetic Island by Forced Reconnection*; Mar. 1991

NIFS-81 K. Takahata, N. Yanagi, T. Mito, J. Yamamoto, O.Motojima and LHDDesign Group, K. Nakamoto, S. Mizukami, K. Kitamura, Y. Wachi, H. Shinohara, K. Yamamoto, M. Shibui, T. Uchida and K. Nakayama, *Design and Fabrication of Forced-Flow Coils as R&D Program for Large Helical Device*; Mar. 1991

NIFS-82 T. Aoki and T. Yabe, *Multi-dimensional Cubic Interpolation for ICF Hydrodynamics Simulation*; Apr. 1991

NIFS-83 K. Ida, S.-I. Itoh, K. Itoh, S. Hidekuma, Y. Miura, H. Kawashima, M. Mori, T. Matsuda, N. Suzuki, H. Tamai, T.Yamauchi and JFT-2M Group, *Density Peaking in the JFT-2M Tokamak Plasma with Counter Neutral Beam Injection* ; May 1991

NIFS-84 A. Iiyoshi, *Development of the Stellarator/Heliotron Research*; May 1991

NIFS-85 Y. Okabe, M. Sasao, H. Yamaoka, M. Wada and J. Fujita, *Dependence of Au^- Production upon the Target Work Function in a Plasma-Sputter-Type Negative Ion Source;* May 1991

NIFS-86 N. Nakajima and M. Okamoto, *Geometrical Effects of the Magnetic Field on the Neoclassical Flow, Current and Rotation in General Toroidal Systems*; May 1991

NIFS-87 S. -I. Itoh, K. Itoh, A. Fukuyama, Y. Miura and JFT-2M Group, *ELMy-H mode as Limit Cycle and Chaotic socillations in Tokamak Plasmas;* May 1991

NIFS-88 N.Matsunami and K.Kitoh, *High Resolution Spectroscopy of H^+ Energy Loss in Thin Carbon Film;* May 1991

NIFS-89 H. Sugama, N. Nakajima and M.Wakatani, *Nonlinear Behavior of Multiple-Helicity Resistive Interchange Modes near Marginally Stable States;* May 1991

NIFS-90 H. Hojo and T.Hatori, *Radial Transport Induced by Rotating RF Fields and Breakdown of Intrinsic Ambipolarity in a Magnetic Mirror*; May 1991

NIFS-91 M. Tanaka, S. Murakami, H. Takamaru and T.Sato, *Macroscale Implicit, Electromagnetic Particle Simulation of Inhomogeneous and Magnetized Plasmas in Multi-Dimensions;* May 1991